IEEE Access
Multidisciplinary | Rapid Review | Open Access Journal

Received May 3, 2022, accepted May 18, 2022, date of publication May 23, 2022, date of current version May 31, 2022.

Digital Object Identifier 10.1109/ACCESS.2022.3176871

Nullforming-Based Precoder for Spectrum Sharing Between HAPS and Terrestrial Mobile Networks

KOJI TASHIRO, (Member, IEEE), KENJI HOSHINO, AND ATSUSHI NAGATE, (Member, IEEE)
SoftBank Corporation, Tokyo 135-0064, Japan

Corresponding author: Koji Tashiro (koji.tashiro@g.softbank.co.jp)

This work was supported in part by the Ministry of Internal Affairs and Communications of Japan through the "Research and Development on Efficient Spectrum Use Technologies for Wireless Communications Systems Using High-Altitude Platform Stations" under Grant JPJ000254.

ABSTRACT Ultra-wide coverage is one of the important concepts of the sixth generation (6G) mobile communications. High-altitude platform stations (HAPSs) have attracted considerable attention as a leading candidate for coverage extension of cellular networks. HAPSs should share a frequency band with terrestrial cellular networks and provide users with mobile communication services using the common frequency band to improve spectral efficiency in service links. However, the signals from HAPS strongly interfere with terrestrial cells in the service area of HAPS, which leads to a considerable deterioration in the system capacity of terrestrial cells. This study proposes a novel two-stage precoding scheme that realizes spectrum sharing between HAPS and terrestrial networks. The proposed scheme mitigates HAPS interference with terrestrial cells using beamforming techniques in phased array antenna systems. In the first stage, nulls are created in directions of terrestrial cells. In the second stage, user-specific beams are formed in directions of users connected to HAPS. Results demonstrate that the proposed scheme improves the signal-to-interference-plus-noise ratio of users in terrestrial cells by up to 10 dB compared with a conventional minimum mean square error (MMSE) precoder without nullforming when the HAPS uses a cylindrical array antenna with 196 elements. Furthermore, for ten terrestrial cells, the proposed scheme achieves 128% of total capacity of the conventional MMSE precoder. Total capacity is defined as the sum capacity of HAPS and all terrestrial cells.

INDEX TERMS HAPS, spectrum sharing, massive MIMO, MU-MIMO, precoding, nullforming, 6G.

I. INTRODUCTION

A. BACKGROUND

Coverage extension to the sky, seas, and everywhere else is one of the most challenging tasks in the sixth generation (6G) mobile communications. In recent years, high-altitude platform stations (HAPSs) have attracted considerable attention as a technology that can extend the service area of cellular networks in 6G and beyond [1], [2]. HAPSs directly provide Internet connections to smartphones and other wireless devices from an unmanned aerial vehicle (UAV) flying in the stratosphere such as an airship, balloon, or a solar-powered aircraft. Originally, HAPSs and related topics were extensively studied in the late 1990s and early 2000s [3]; however, they did not reach commercialization because of insufficient performances of UAVs. In the last 20 years, flight performances of UAVs have drastically improved owing to significant advances in solar power and battery technologies, which makes it possible to develop HAPS systems that satisfy the strict requirements placed for commercial mobile communication services. For example, SoftBank Corp.'s HAPSMobile Inc. and Alphabet's Loon LLC succeeded in the world's first delivery of long-term evolution (LTE) connectivity from a fixed-wing autonomous aircraft with a wingspan of 80 m, named Sunglider, in the stratosphere in 2020 [4]. Airbus developed a solar-electric UAV with a wingspan of 25 m, known as Zephyr S, and they have achieved 36 days of stratospheric flight in 2021 with a total of 2,435 flight hours [5].

HAPSs are expected to be used in the following two major cases: to provide emergency communication services over disaster-hit areas and to increase the coverage area of cellular networks. Achieving a larger coverage with a small number

The associate editor coordinating the review of this manuscript and approving it for publication was Jiankang Zhang.

of UAVs is important to provide users with mobile communication services at a low cost as an aircraft's price and a maintenance cost are considerably high. Considering the use cases of HAPSs and their costs, the service area provided by a single aircraft should be extended as much as possible. Long-range coverage of up to 100 km is supported in the fourth (4G) and fifth generation (5G) mobile communications. This study targets the HAPS service area with a radius of 100 km.

In communications between HAPS and users, called service links, it is possible for HAPSs to use massive multiple-input multiple-output (MIMO) techniques with a large-scale array antenna to compensate for severe path loss caused by long-range propagation. Moreover, multiuser MIMO (MU-MIMO) techniques can be used to enhance system capacity, where a group of users are spatially multiplexed on a single time-frequency resource simultaneously [6], [7]. In general, a single HAPS can cover an even larger area than the base station (BS) used in terrestrial cellular systems. Hence, even in less-populated areas, multiple terrestrial BSs are located in the service area of a single HAPS, where some or all of them would be in service using the same frequency band as the HAPS. Currently, the 2 GHz band is the only global band that has already been identified for HAPS communications in the service link. The upcoming world radiocommunication conference 2023 (WRC-23) plans to discuss the usage of certain frequency bands below 2.7 GHz [8]. Moreover, the 2 GHz band is commonly used for terrestrial mobile networks. The HAPS and terrestrial BSs should use the same frequency band to achieve high spectral efficiency. However, the signals from HAPS interfere with users in terrestrial cells. In particular, HAPSs with a large-scale array antenna create high-gain beams in directions of users located in its service area. The high-gain beams improve communication quality of users connected to the HAPS; however, they strongly interfere with users attached to each terrestrial cell, which can seriously degrade the system capacity of terrestrial mobile networks.

B. RELATED WORK

Unlike extensive studies on capacity enhancement and theoretical analysis of HAPSs [6], [7], [9], [10], few studies have specifically addressed the spectrum sharing between HAPSs and 4G or 5G networks on the ground.

In [11], Peng *et al*. have proposed a method to provide specialist users in a service area with gigabit wireless communication links using multiple spot beams from HAPS. The spot beams created by highly directional antennas effectively suppress the interference from HAPS to terrestrial cells, which makes it possible to share a common frequency band with terrestrial networks. However, this approach requires the same number of physical antennas as specialist users. It would be difficult for HAPSs to provide commercial 4G or 5G services using this approach because a single HAPS accommodates much more users than antennas. A similar idea for multiple HAPSs cases has been presented in [12].

In [13], [14], Konishi *et al*. have proposed a carrier aggregation (CA)-based spectrum sharing method, where terrestrial BSs use two or more frequency bands (e.g., 900 MHz and 2 GHz), and a HAPS shares one of these bands (e.g., 2 GHz) with terrestrial BSs. When a user is located close to the center of a terrestrial cell, the received power of signals from the cell becomes greater than that from HAPS. In such a case, the user can ignore the interference from HAPS and activate the CA scheme that combines both the shared and unshared bands. When a user is located in proximity around the boundary of a terrestrial cell, only the unshared band can be used. This CA-based approach is the spectrum sharing technique performed on terrestrial networks, and it cannot reduce the interference on the shared band. Thus, it cannot be a radical solution to the co-channel interference from HAPS.

In [15], Lim *et al*. have presented a novel precoding technique for MU-MIMO systems to eliminate interference from a terrestrial BS to earth stations used for fixed satellite service. They have modified a unitary precoding scheme to support null steering from a terrestrial BS to earth stations. However, this approach also cannot be directly applied to spectrum sharing between HAPS and terrestrial BSs because it supports only uniform linear arrays (ULAs), in which vertical or horizontal ULAs create only elevation or azimuth nulls, respectively. Unlike firmly fixed terrestrial BSs, the aircraft of HAPSs moves and rotates while flying in the stratosphere. Therefore, it is necessary for HAPSs to adaptively and jointly control the elevation and azimuth angles of beams and nulls; ULAs do not satisfy this important requirement.

In [16], Srinivasan *et al*. have demonstrated multiple beamforming algorithms designed for planar arrays with thousands of antenna elements, targeting millimeter-wave HAPS systems. In [17], Hu *et al*. have examined an interference model for HAPS massive MIMO systems with a planar array. Planar array antennas are capable of three-dimensional (3D) adaptive beamforming; however, their coverage radius is limited to only 20–60 km [6], [7].

In [18], Ananth *et al*. have examined the effect of interference from Loon's HAPS, where LTE signals are transmitted from HAPS with a single antenna using a frequency band below 1 GHz. The authors demonstrated that signal-to-interference-plus-noise ratio (SINR) decreases around terrestrial cells in exchange for substantial coverage extension by HAPS. Additional studies on spectrum sharing for HAPSs have been reported in [19], [20].

C. CONTRIBUTIONS

The final aim of this study is to develop a HAPS system that realizes spectrum sharing with terrestrial networks, where the target coverage radius of a single HAPS is 100 km. In our previous work [9], we have discussed the array antenna structure to achieve ultra-wide coverage using HAPSs and have proposed a massive MU-MIMO system that exploits a cylindrical array antenna. However, coexistence with terrestrial BSs was not considered in that study. This study expands the prior discussion to include spectrum sharing with terrestrial

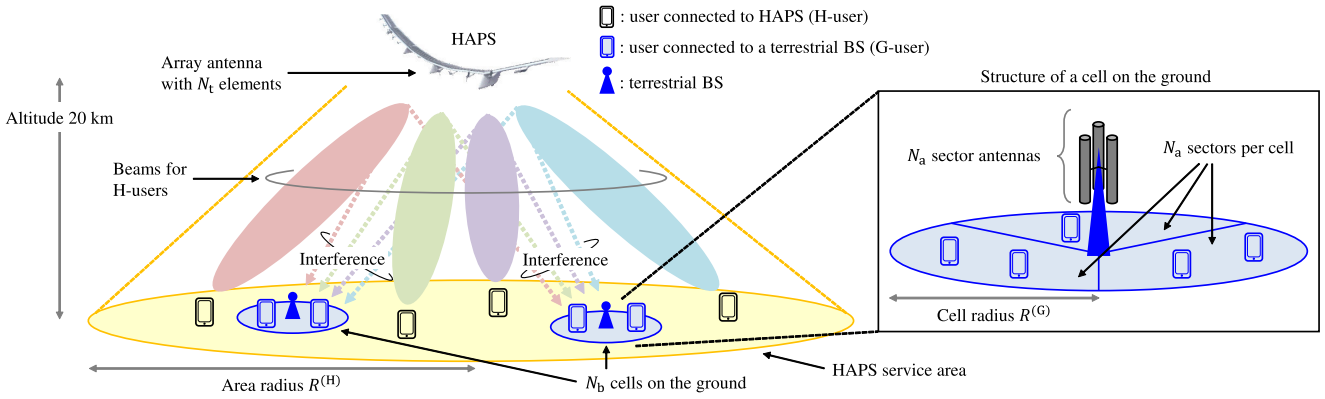

FIGURE 1. System model where a single HAPS with massive MU-MIMO and multiple sectorized cells on the ground use a common frequency band.

networks. In particular, we focus only on downlink communications because co-channel interference is more critical in downlink than in uplink. As a target area for HAPS services, we select a vast area with a scattering of small cities, villages, or settlements with large coverage holes because of sparsely deployed terrestrial BSs. The primary contributions of this study are summarized as follows:

- A system model for coexisting HAPS and terrestrial BSs has been introduced, where a single HAPS using massive MU-MIMO and multiple sectorized cells on the ground share a common frequency band to communicate with their users.
- A novel two-stage precoding scheme for massive MU-MIMO systems has been proposed, which adaptively creates nulls in directions of terrestrial BSs and generates high-gain beams in directions of users. The proposed precoding scheme with a cylindrical array antenna supports 3D nullforming and beamforming.
- Based on the proposed scheme mentioned above, the following two different precoders have been proposed: one is a nullforming-based zero-forcing (ZF) precoder; the other is a nullforming-based minimum mean square error (MMSE) precoder. Both of them are similar in that they create nulls in directions of terrestrial BSs in the first stage. However, they apply different beamforming algorithms to generate user-specific beams in the second stage.
- In-depth evaluations have been performed to clarify the effectiveness of the proposed precoders under coexistence situations in terms of radiation power patterns of an array antenna, SINR per user, and system capacity. The proposed precoders are compared with a conventional MMSE precoder without nullforming.

D. PAPER ORGANIZATION

The rest of this paper is structured as follows. Section II provides an overview of the coexistence model, where multiple terrestrial BSs are located in the service area of a single HAPS. Section III proposes the nullforming-based two-stage precoding scheme that realizes spectrum sharing between HAPS and terrestrial cells. Section IV provides simulations details to evaluate the effectiveness of the proposed scheme. Section V presents the simulation results and compares the performances of the proposed precoders with those of the conventional MMSE precoder without nullforming. Finally, Section VI concludes this study.

E. NOTATIONS

The following notations will be used throughout this study. Superscripts $(\cdot)^T$, $(\cdot)^H$, and $(\cdot)^{-1}$ represent the matrix transpose, Hermitian transpose, and matrix inverse, respectively. $\mathbf{I}_m$ denotes an $m \times m$ identity matrix, and $\mathbf{O}_{m,n}$ denotes an $m \times n$ matrix with zero entries. $\mathrm{j} = \sqrt{-1}$ denotes the imaginary unit, $\mathbb{C}$ denotes the set of complex numbers, $||\cdot||$ denotes the L-2 norm, and $|\cdot|$ denotes the absolute value of a complex number or the cardinality of a set. $E[\cdot]$ denotes the ensemble average, and $\min(a, b)$ returns the smaller of two real numbers a and b.

II. DOWNLINK COEXISTENCE MODEL FOR A HAPS AND TERRESTRIAL NETWORKS

A. SYSTEM MODEL

Fig. 1 shows the system model considered in this study, where N_b terrestrial BSs are located in the service area of a HAPS. A single HAPS flying at an altitude of 20 km covers a circular area with a radius $R^{(H)}$, and the cell radius of each terrestrial BS is $R^{(G)}$ ($R^{(G)} \ll R^{(H)}$). For simplicity, every user has a single omnidirectional antenna. It is assumed that users in a terrestrial cell are attached to a terrestrial BS, and those inside the HAPS service area but outside the terrestrial cells are connected to HAPS. To distinguish these two types of users, the users connected to HAPS and those connected to terrestrial BSs are referred to as "H-users" and "G-users," respectively. A large-scale array antenna with N_t elements is mounted at the bottom of the aircraft to support massive MU-MIMO communications. Each terrestrial BS is equipped with N_a directional antennas to develop a cell with N_a sectors. The configuration parameters of all terrestrial BSs are equal, but

their locations differ. Note that HAPS and all terrestrial BSs share a single common frequency band.

In downlink transmissions, the HAPS generates different directional beams, which do not interfere with each other, using massive MU-MIMO techniques. Therefore, N_{u} H-users are served on a single time-frequency resource at once. Here, let $\mathcal{H} = \{1, \cdots, N_{\mathrm{u}}\}$ be the index set of H-users served on a single time-frequency resource, and let $x_u^{(\mathcal{H})}$ be the symbol transmitted to H-user $u \in \mathcal{H}$. The transmit power of $x_u^{(\mathcal{H})}$ is defined as $p_u^{(\mathcal{H})} = E\left[\left|x_u^{(\mathcal{H})}\right|^2\right]$. The precoding weight vector applied to $x_u^{(\mathcal{H})}$ is denoted by $\mathbf{w}_u \in \mathbb{C}^{N_{\mathrm{t}} \times 1}$. The channel vector between the HAPS and H-user u is denoted by $\mathbf{h}_u^{(\mathcal{H})} \in \mathbb{C}^{1 \times N_{\mathrm{t}}}$. Then, the received signal at H-user $u \in \mathcal{H}$ can be written as follows:

$$r_u^{(\mathcal{H})} = \mathbf{h}_u^{(\mathcal{H})} \mathbf{w}_u x_u^{(\mathcal{H})} + \sum_{i=1, i \neq u}^{N_{\mathrm{u}}} \mathbf{h}_u^{(\mathcal{H})} \mathbf{w}_i x_i^{(\mathcal{H})} + n_u^{(\mathcal{H})}, \quad (1)$$

where the first term is the desired signal, the second term is the interference of all the other H-users, and $n_u^{(\mathcal{H})}$ is the additive white Gaussian noise (AWGN) at the receiver side.

Single-stream transmission is assumed in the downlink communications between terrestrial BSs and G-users. A total of $N_{\mathrm{a}}N_{\mathrm{b}}$ G-users can be served on a single time-frequency resource simultaneously because $N_{\mathrm{a}}N_{\mathrm{b}}$ sectors exist on the ground. Here, let $\mathcal{G} = \{1, \cdots, N_{\mathrm{a}}N_{\mathrm{b}}\}$ be the index set of G-users served on a single time-frequency resource. Note that G-user $s \in \mathcal{G}$ belongs to sector s. In the same manner as H-users, let $x_s^{(\mathcal{G})}$ be the symbol transmitted to G-user s, where the transmit power of $x_s^{(\mathcal{G})}$ is defined as $p_s^{(\mathcal{G})} = E\left[\left|x_s^{(\mathcal{G})}\right|^2\right]$. Letting $g_{s,j}^{(\mathcal{G})}$ be the channel coefficient between sector j and G-user s, the received signal at G-user $s \in \mathcal{G}$ can be written as follows:

$$r_s^{(\mathcal{G})} = g_{s,s}^{(\mathcal{G})} x_s^{(\mathcal{G})} + \sum_{j=1, j \neq s}^{N_{\mathrm{a}}N_{\mathrm{b}}} g_{s,j}^{(\mathcal{G})} x_j^{(\mathcal{G})} + n_s^{(\mathcal{G})}, \quad (2)$$

where the first term is the desired signal, the second term is the other sectors' interference, and $n_s^{(\mathcal{G})}$ is the AWGN at the receiver side.

Because the HAPS and terrestrial BSs use the same frequency band, a co-channel interference term should be added to (1) and (2). Considering the interference from all sectors on the ground, the received signal at H-user $u \in \mathcal{H}$, described in (1), can be rewritten as follows:

$$y_u^{(\mathcal{H})} = r_u^{(\mathcal{H})} + \sum_{j=1}^{N_{\mathrm{a}}N_{\mathrm{b}}} g_{u,j}^{(\mathcal{H})} x_j^{(\mathcal{G})}, \quad (3)$$

where $g_{u,j}^{(\mathcal{H})}$ is the channel coefficient between sector j and H-user u. Similarly, considering the interference from the HAPS, the received signal at G-user $s \in \mathcal{G}$, described in (2), can be rewritten as follows:

$$y_s^{(\mathcal{G})} = r_s^{(\mathcal{G})} + \sum_{i=1}^{N_{\mathrm{u}}} \mathbf{h}_s^{(\mathcal{G})} \mathbf{w}_i x_i^{(\mathcal{H})}, \quad (4)$$

where $\mathbf{h}_s^{(\mathcal{G})}$ is the channel vector between the HAPS and G-user s. Finally, (3) and (4) are expressed in the following matrix form:

$$\mathbf{y}^{(\mathcal{H})} = \underbrace{\mathbf{H}^{(\mathcal{H})}\mathbf{W}\mathbf{x}^{(\mathcal{H})}}_{\text{desired signal}} + \underbrace{\mathbf{G}^{(\mathcal{H})}\mathbf{x}^{(\mathcal{G})}}_{\text{interference from BSs}} + \mathbf{n}^{(\mathcal{H})}, \quad (5)$$

$$\mathbf{y}^{(\mathcal{G})} = \underbrace{\mathbf{G}^{(\mathcal{G})}\mathbf{x}^{(\mathcal{G})}}_{\text{desired signal}} + \underbrace{\mathbf{H}^{(\mathcal{G})}\mathbf{W}\mathbf{x}^{(\mathcal{H})}}_{\text{interference from HAPS}} + \mathbf{n}^{(\mathcal{G})}. \quad (6)$$

Letting $\mathcal{N}$ be either $\mathcal{H}$ or $\mathcal{G}$, the vectors and matrices in (5) and (6) are defined as follows:

$$\mathbf{y}^{(\mathcal{N})} = \left[y_1^{(\mathcal{N})}, \cdots, y_{|\mathcal{N}|}^{(\mathcal{N})}\right]^T \in \mathbb{C}^{|\mathcal{N}| \times 1}, \quad (7)$$

$$\mathbf{H}^{(\mathcal{N})} = \left[\left(\mathbf{h}_1^{(\mathcal{N})}\right)^T, \cdots, \left(\mathbf{h}_{|\mathcal{N}|}^{(\mathcal{N})}\right)^T\right]^T \in \mathbb{C}^{|\mathcal{N}| \times N_{\mathrm{t}}}, \quad (8)$$

$$\mathbf{G}^{(\mathcal{N})} = \begin{bmatrix} g_{1,1}^{(\mathcal{N})} & \cdots & g_{1,N_{\mathrm{a}}N_{\mathrm{b}}}^{(\mathcal{N})} \\ \vdots & \ddots & \vdots \\ g_{|\mathcal{N}|,1}^{(\mathcal{N})} & \cdots & g_{|\mathcal{N}|,N_{\mathrm{a}}N_{\mathrm{b}}}^{(\mathcal{N})} \end{bmatrix} \in \mathbb{C}^{|\mathcal{N}| \times N_{\mathrm{a}}N_{\mathrm{b}}}, \quad (9)$$

$$\mathbf{W} = \left[\mathbf{w}_1, \cdots, \mathbf{w}_{N_{\mathrm{u}}}\right] \in \mathbb{C}^{N_{\mathrm{t}} \times N_{\mathrm{u}}}, \quad (10)$$

$$\mathbf{x}^{(\mathcal{N})} = \left[x_1^{(\mathcal{N})}, \cdots, x_{|\mathcal{N}|}^{(\mathcal{N})}\right]^T \in \mathbb{C}^{|\mathcal{N}| \times 1}, \quad (11)$$

$$\mathbf{n}^{(\mathcal{N})} = \left[n_1^{(\mathcal{N})}, \cdots, n_{|\mathcal{N}|}^{(\mathcal{N})}\right]^T \in \mathbb{C}^{|\mathcal{N}| \times 1}. \quad (12)$$

B. CONVENTIONAL PRECODING AT THE HAPS SIDE

Downlink MU-MIMO systems require precoding techniques to simultaneously produce multiple user-specific beams and suppress the interference between them. This type of interference is known as inter-user interference (IUI) in MU-MIMO communications, and many precoders that mitigate the IUI have been proposed. Among them, MMSE is one of the most fundamental and well-used linear precoding algorithms [21], and its precoding weight matrix is given by

$$\mathbf{W}^{(\mathrm{MMSE})} = f_{\mathrm{n}}\left(\left(\mathbf{H}^{(\mathcal{H})}\right)^H \mathbf{R}^{-1}\right), \quad (13)$$

$$\mathbf{R} = \mathbf{H}^{(\mathcal{H})}\left(\mathbf{H}^{(\mathcal{H})}\right)^H + \frac{P_{\mathrm{n}}N_{\mathrm{u}}}{P_{\mathrm{t}}}\mathbf{I}_{N_{\mathrm{u}}}, \quad (14)$$

where $f_{\mathrm{n}}(\cdot)$ is the function that normalizes the columns of an input matrix, P_{n} is the noise power at the receiver side, and $P_{\mathrm{t}} = \sum_{u=1}^{N_{\mathrm{u}}} p_u^{(\mathcal{H})}$ is the total transmit power allocated to all H-users. The second term on the right side of (14) is the regularization factor to avoid the inversion of an ill-conditioned matrix. In this study, the perfectly estimated channel matrix, or error-free $\mathbf{H}^{(\mathcal{H})}$, is assumed to be available at the HAPS side. In practical communications, HAPSs can estimate $\mathbf{H}^{(\mathcal{H})}$ using the reciprocity of uplink and downlink channels [22] or directly acquire it through explicit channel state information (CSI) feedback from each H-user [23]. For mobile H-users, HAPSs estimate or acquire $\mathbf{H}^{(\mathcal{H})}$ more frequently to update user-specific beams. This CSI update process is common in terrestrial BSs and not specific to HAPSs. Note that evaluations in the presence of channel estimation errors are outside the scope of this study.

C. CHANNEL MODELS

Fig. 2 shows the positional relation between HAPS, terrestrial BSs, and their users. As shown in Fig. 2, in general, the elevation angle from users to HAPS is much larger than that from users to a terrestrial BS. Thus, this study assumes line-of-sight (LoS) channels between HAPS and terrestrial users and non-line-of-sight (NLoS) channels between a terrestrial BS and users.

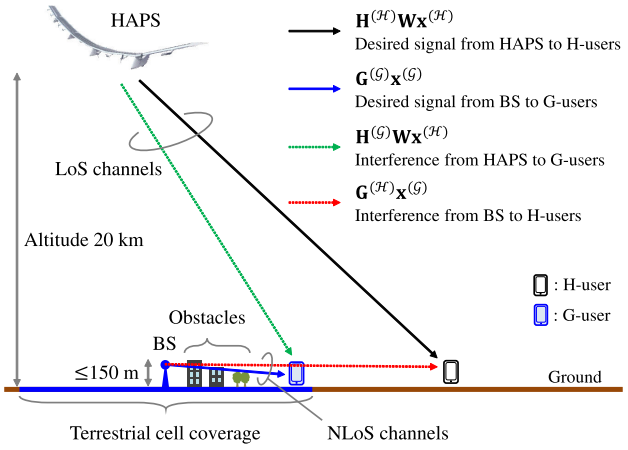

FIGURE 2. Positional relation between HAPS, terrestrial BSs, and their users. Solid and dashed lines indicate desired and interference paths, respectively.

In downlink communications between HAPS and outdoor users in a broad area with a flat surface, the probability of LoS propagation is considerably high because there are few obstacles between outdoor users and aircraft flying in the stratosphere [1], [2]. Therefore, this study simply assumes pure LoS channels between HAPS and users on the ground. Let $\mathcal{N}$ be either $\mathcal{H}$ or $\mathcal{G}$, and let $h_{n,t}^{(\mathcal{N})}$ be the channel coefficient modeled by the direct path between user $n \in \mathcal{N}$ and element $t \in \{1, \cdots, N_\mathrm{t}\}$ of an array antenna. The channel vector between the HAPS and user n is defined as $\mathbf{h}_n^{(\mathcal{N})} = \left[h_{n,1}^{(\mathcal{N})}, \cdots, h_{n,N_\mathrm{t}}^{(\mathcal{N})}\right]$, where $h_{n,t}^{(\mathcal{N})}$ can be modeled as follows [24]:

$$h_{n,t}^{(\mathcal{N})} = \beta_\mathrm{e}\left(\theta_{n,t}^{(\mathcal{N})}, \phi_{n,t}^{(\mathcal{N})}\right) o_n^{(\mathcal{N})} l_{n,t}^{(\mathcal{N})} \rho_{n,t}^{(\mathcal{N})}, \tag{15}$$

$$l_{n,t}^{(\mathcal{N})} = \left(\frac{4\pi}{\lambda} d_{n,t}^{(\mathcal{N})}\right)^{-1}, \tag{16}$$

$$\rho_{n,t}^{(\mathcal{N})} = \exp\left(\mathrm{j}\frac{2\pi}{\lambda} d_{n,t}^{(\mathcal{N})}\right). \tag{17}$$

The function $\beta_\mathrm{e}(\theta, \phi)$ in (15) returns the radiation pattern of a single antenna element at elevation θ and azimuth ϕ, and $\theta_{n,t}^{(\mathcal{N})} \in [-90°, 90°]$ and $\phi_{n,t}^{(\mathcal{N})} \in [-180°, 180°]$ denote the elevation and azimuth angles from the t-th element to user n, respectively. In (15), $o_n^{(\mathcal{N})}$ denotes the receive antenna gain of user n. In (16) and (17), λ denotes the carrier wavelength, and $l_{n,t}^{(\mathcal{N})}$, $\rho_{n,t}^{(\mathcal{N})}$, and $d_{n,t}^{(\mathcal{N})}$ denote the free-space path loss coefficient, the phase rotation, and the distance between element t and user n, respectively.

In downlink communications between a terrestrial BS and users, a direct path can be easily blocked by some obstacles, including buildings, trees, and mountains, because the typical height of a terrestrial BS is not more than 150 m, as shown in Fig. 2. Hence, this study assumes NLoS channels between a terrestrial BS and users. Unlike the adaptive precoding at the HAPS side, a fixed beam pattern is assumed for N_a sector antennas of each terrestrial BS. Letting $\mathcal{N}$ be either $\mathcal{H}$ or $\mathcal{G}$, the channel coefficient between sector $j \in \mathcal{G}$ and G-user $n \in \mathcal{N}$ can be modeled as follows:

$$g_{n,j}^{(\mathcal{N})} = \beta_\mathrm{s}\left(\chi_{n,j}^{(\mathcal{N})}, \psi_{n,j}^{(\mathcal{N})}\right) o_n^{(\mathcal{N})} \alpha_{n,j}^{(\mathcal{N})} z_{n,j}^{(\mathcal{N})}, \tag{18}$$

in which the function $\beta_\mathrm{s}(\theta, \phi)$ returns the radiation pattern of a sector antenna at elevation θ and azimuth ϕ, and $\chi_{n,j}^{(\mathcal{N})} \in [-90°, 90°]$ and $\psi_{n,j}^{(\mathcal{N})} \in [-180°, 180°]$ denote the elevation and azimuth angles from sector j to user n, respectively. In (18), $\alpha_{n,j}^{(\mathcal{N})}$ denotes the path loss coefficient between sector j and user n. In this study, $\alpha_{n,j}^{(\mathcal{N})}$ is calculated using the COST-231 Hata model for suburban areas [25], [26]. In (18), $z_{n,j}^{(\mathcal{N})}$ is the Rayleigh fading coefficient between sector j and user n, which is given by a circularly symmetric complex Gaussian random valuable with zero mean and unit variance.

III. PROPOSED PRECODING SCHEME

A. MAIN IDEA

As shown in Fig. 2, NLoS propagation scenarios have been assumed between terrestrial BSs and users. The interference from terrestrial BSs to H-users, represented by $\mathbf{G}^{(\mathcal{H})}\mathbf{x}^{(\mathcal{G})}$ in (5), is expected to be sufficiently small when H-users are away from terrestrial BSs. In general, terrestrial cells are carefully designed to suppress inter-cell interference by adjusting the down tilt angle of each sector beam or antenna. Thus, even for coexisting HAPS and terrestrial BSs, there is no need to deal with the interference from terrestrial BSs to H-users. However, the interference from HAPS to G-users, denoted by $\mathbf{H}^{(\mathcal{G})}\mathbf{W}\mathbf{x}^{(\mathcal{H})}$ in (6), is too large to ignore because of LoS-dominant propagation scenarios in which transmit signals from the HAPS strongly interfere with communications between terrestrial BSs and G-users. Consequently, the downlink signals from HAPS to H-users can deteriorate the communication performance of terrestrial networks.

This study proposes a novel two-stage precoding scheme for HAPS systems to suppress the interference to G-users. In the first stage, nulls are formed in directions of terrestrial BSs. In the second stage, user-specific beams for H-users are then formed. To realize this two-stage control, the proposed scheme factorizes the precoding weight matrix in (10) into the following two matrices:

$$\mathbf{W} = \mathbf{W}_\mathrm{NF}\mathbf{W}_\mathrm{BF}, \tag{19}$$

where $\mathbf{W}_\mathrm{NF} \in \mathbb{C}^{N_\mathrm{t} \times M}$ and $\mathbf{W}_\mathrm{BF} \in \mathbb{C}^{M \times N_\mathrm{u}}$ represent the nullforming and beamforming matrices, respectively, and M

represents the number of elements used to produce user-specific beams. As described in (19), the proposed scheme separately controls nulls and user-specific beams in different stages. Once nulls are formed in directions of terrestrial BSs by $\mathbf{W}_{\mathrm{NF}}$ in the first stage, the directions of null points do not change even after the second stage regardless of $\mathbf{W}_{\mathrm{BF}}$. In this manner, the proposed scheme realizes the spectrum sharing between HAPS and terrestrial mobile networks by cancelling out the interference from the HAPS to terrestrial BSs. Note that the proposed scheme targets only single-sector HAPSs; it cannot be directly applied to multi-sector HAPSs. For handling multi-sector scenarios, the proposed scheme requires modifications to suppress inter-sector interference.

B. NULLFORMING FOR TERRESTRIAL BASE STATIONS

In general, an array antenna with N_{t} elements has a total of $N_{\mathrm{t}}-1$ degrees of freedom; it can form up to $N_{\mathrm{t}}-1$ nulls at once. To cancel out the interference from HAPS to G-users, denoted by $\mathbf{H}^{(\mathcal{G})}\mathbf{W}\mathbf{x}^{(\mathcal{H})}$ in (6), it is necessary to create $N_{\mathrm{a}}N_{\mathrm{b}}$ null points by $\mathbf{W}_{\mathrm{NF}}$. In other words, $\mathbf{W}_{\mathrm{NF}}$ should satisfy the following condition:

$$\mathbf{H}^{(\mathcal{G})}\mathbf{W}_{\mathrm{NF}} = \mathbf{O}_{N_{\mathrm{a}}N_{\mathrm{b}},M}. \tag{20}$$

In this case, a total of $N_{\mathrm{a}}N_{\mathrm{b}}$ degrees of freedom are used in the nullforming process at the first stage; i.e., the remaining number of elements used in the beamforming process at the second stage is expressed as $M = N_{\mathrm{t}} - N_{\mathrm{a}}N_{\mathrm{b}}$. To generate high-gain beams for H-users in the second stage, it is better to minimize the number of null points created in the first stage or equivalently maximize M.

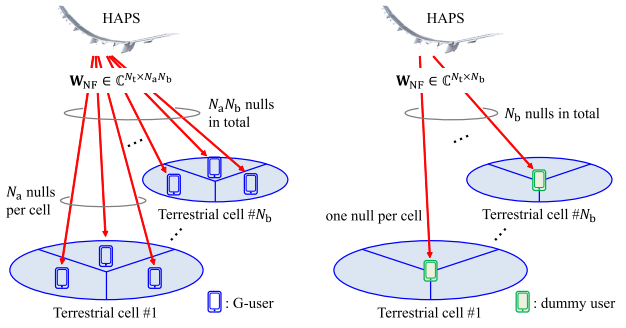

(a) Nullforming in (20) (b) Nullforming in (21)

FIGURE 3. Graphical interpretation of the difference in nullforming strategy between (20) and (21).

Fig. 3(a) shows the graphical interpretation of (20). In Fig. 3(a), the nullforming targets are G-users in all $N_{\mathrm{a}}N_{\mathrm{b}}$ sectors, where a single null corresponds to a single G-user (N_{a} nulls per cell). However, a single null is wide enough to cover the entire area of a cell because the distance from the aircraft to a terrestrial BS is sufficiently larger than the cell diameter. Therefore, the number of null points can be reduced by changing the nullforming targets to each terrestrial BS rather than each G-user. In the proposed scheme, the HAPS considers each terrestrial BS as a dummy user with a single antenna element and creates nulls in directions of each dummy user, as shown in Fig. 3(b). Fig. 3(b) necessitates only N_{b} nulls, whereas Fig. 3(a) requires $N_{\mathrm{a}}N_{\mathrm{b}}$ nulls. Letting $\mathcal{B} = \{1,\cdots,N_{\mathrm{b}}\}$ be the index set of terrestrial BSs or dummy users, the nullforming condition in (20) is modified as follows:

$$\mathbf{H}^{(\mathcal{B})}\mathbf{W}_{\mathrm{NF}} = \mathbf{O}_{N_{\mathrm{b}},M}, \tag{21}$$

where $\mathbf{H}^{(\mathcal{B})} = \left[\left(\mathbf{h}_1^{(\mathcal{B})}\right)^T,\cdots,\left(\mathbf{h}_{N_{\mathrm{b}}}^{(\mathcal{B})}\right)^T\right]^T \in \mathbb{C}^{N_{\mathrm{b}}\times N_{\mathrm{t}}}$, and $\mathbf{h}_b^{(\mathcal{B})}$ is the channel vector between the HAPS and dummy user $b \in \mathcal{B}$. These dummy users are completely the same as H- or G-users except that they are always located at the center of each cell. Hence, $\mathbf{h}_b^{(\mathcal{B})}$ can be obtained by replacing $n \in \mathcal{N}$ with $b \in \mathcal{B}$ in (15)–(17).

The nullforming scheme in Fig. 3(a) requires information about user scheduling and G-users' locations from all terrestrial BSs. However, it would be practically difficult to satisfy this requirement because the real-time feedback of scheduling and location information drastically increases the traffic on feeder links, particularly when the number of BSs is large. This is a serious drawback of the nullforming strategy in Fig. 3(a). Furthermore, the nullforming scheme in Fig. 3(b) requires only the locations of all terrestrial BSs or dummy users within its service area for calculating $\mathbf{H}^{(\mathcal{B})}$ as LoS channels modeled in (15)–(17) are characterized only by the positional relation between an array antenna and each user. In practice, the HAPS system can regularly update the list of terrestrial BSs and obtain the latest information about their location.

Letting $\mathbf{W}_{\mathrm{NF}}^{(\mathcal{B})}$ be the nullforming mtarix that satisfies (21), $\mathbf{W}_{\mathrm{NF}}^{(\mathcal{B})}$ is obtained by applying the following singular value decomposition to $\mathbf{H}^{(\mathcal{B})}$:

$$\mathbf{H}^{(\mathcal{B})} = \mathbf{U}^{(\mathcal{B})}\left[\Sigma^{(\mathcal{B})}\ \mathbf{O}_{N_{\mathrm{b}},N_{\mathrm{t}}-N_{\mathrm{b}}}\right]\left(\mathbf{V}^{(\mathcal{B})}\right)^H, \tag{22}$$

where $\mathbf{U}^{(\mathcal{B})} \in \mathbb{C}^{N_{\mathrm{b}}\times N_{\mathrm{b}}}$ represents the left singular matrix, $\Sigma^{(\mathcal{B})} \in \mathbb{C}^{N_{\mathrm{b}}\times N_{\mathrm{b}}}$ is the diagonal matrix whose diagonal entries are the singular values of $\mathbf{H}^{(\mathcal{B})}$, and $\mathbf{V}^{(\mathcal{B})} \in \mathbb{C}^{N_{\mathrm{t}}\times N_{\mathrm{t}}}$ represents the right singular matrix. As described in (22), the columns of $\mathbf{V}^{(\mathcal{B})}$ corresponding to $\mathbf{O}_{N_{\mathrm{b}},N_{\mathrm{t}}-N_{\mathrm{b}}}$, denoted by $\left\{\mathbf{v}_{N_{\mathrm{b}}+1}^{(\mathcal{B})},\cdots,\mathbf{v}_{N_{\mathrm{t}}}^{(\mathcal{B})}\right\}$, are the null space of $\mathbf{H}^{(\mathcal{B})}$, and $\mathbf{W}_{\mathrm{NF}}^{(\mathcal{B})}$ is finally obtained by selecting M vectors from them. The details on M will be provided later.

C. BEAMFORMING FOR H-USERS

After the nullforming process in the first stage, user-specific beams for H-users are formed in the second stage. Regarding the nullforming as part of propagation channels, conventional precoding algorithms for downlink MU-MIMO systems can be used. In other words, $\mathbf{W}_{\mathrm{BF}}$ in (19) can be calculated by applying a conventional precoding scheme to $\tilde{\mathbf{H}}$, where $\tilde{\mathbf{H}} = \mathbf{H}^{(\mathcal{H})}\mathbf{W}_{\mathrm{NF}}^{(\mathcal{B})} \in \mathbb{C}^{N_{\mathrm{u}}\times M}$ denotes the composite channel matrix that comprises the original channel and nullforming matrices.

This study uses the following two major and fundamental beamforming criteria to calculate $\mathbf{W}_{\mathrm{BF}}$: ZF [27] and MMSE in (13). The former completely removes the IUI, whereas the latter considers both the IUI and noise level. The precoding weight matrices based on ZF and MMSE criteria are given by

$$\mathbf{W}_{\mathrm{BF}}^{(\mathrm{ZF})} = \tilde{\mathbf{H}}^{H}\left(\tilde{\mathbf{H}}\tilde{\mathbf{H}}^{H}\right)^{-1}, \tag{23}$$

$$\mathbf{W}_{\mathrm{BF}}^{(\mathrm{MMSE})} = \tilde{\mathbf{H}}^{H}\left(\tilde{\mathbf{H}}\tilde{\mathbf{H}}^{H} + \frac{P_{\mathrm{n}}N_{\mathrm{u}}}{P_{\mathrm{t}}}\mathbf{I}_{N_{\mathrm{u}}}\right)^{-1}. \tag{24}$$

The overall precoding matrices that include nullforming and beamforming are given by

$$\mathbf{W}^{(\mathrm{ZF})} = f_{\mathrm{n}}\left(\mathbf{W}_{\mathrm{NF}}^{(\mathcal{B})}\mathbf{W}_{\mathrm{BF}}^{(\mathrm{ZF})}\right), \tag{25}$$

$$\mathbf{W}^{(\mathrm{MMSE})} = f_{\mathrm{n}}\left(\mathbf{W}_{\mathrm{NF}}^{(\mathcal{B})}\mathbf{W}_{\mathrm{BF}}^{(\mathrm{MMSE})}\right). \tag{26}$$

Finally, we have

$$\mathbf{H}^{(\mathcal{B})}\mathbf{W}^{(\mathrm{ZF})} = \mathbf{H}^{(\mathcal{B})}\mathbf{W}^{(\mathrm{MMSE})} = \mathbf{O}_{N_{\mathrm{b}},N_{\mathrm{u}}}. \tag{27}$$

A single null is wide enough to cover the entire area of a cell; thus, we have

$$\mathbf{H}^{(\mathcal{G})}\mathbf{W}^{(\mathrm{ZF})} \approx \mathbf{H}^{(\mathcal{G})}\mathbf{W}^{(\mathrm{MMSE})} \approx \mathbf{O}_{N_{\mathrm{a}}N_{\mathrm{b}},N_{\mathrm{u}}}. \tag{28}$$

In this manner, the proposed precoders mitigate the interference from HAPS to G-users and generate user-specific beams for H-users. The proposed scheme is independent of array geometry and functions with any type of array antenna. The proposed scheme requires only the CSI between HAPS and H-users, denoted by $\mathbf{H}^{(\mathcal{H})}$, and the locations of all terrestrial BSs. As mentioned in Section II-B, the acquisition of $\mathbf{H}^{(\mathcal{H})}$ is a common assumption in MU-MIMO communications. In addition, the locations of terrestrial BSs can be easily obtained by accessing the database of terrestrial BSs via feeder links.

D. PRECODER ARCHITECTURE

Fig. 4 describes a block diagram of the proposed precoder at the HAPS side. In Fig. 4, $\mathbf{W}_{\mathrm{NF}}$ forms N_{b} nulls to cancel out the interference to terrestrial cells, and $\mathbf{W}_{\mathrm{BF}}$ creates $N_{\mathrm{u}}-1$ nulls to remove the IUI. As explained previously, an array antenna with N_{t} elements can create $N_{\mathrm{t}}-1$ nulls in total. Therefore, $N_{\mathrm{b}}+N_{\mathrm{u}} \le N_{\mathrm{t}}$ should be satisfied for successful nullforming and beamforming in the proposed scheme.

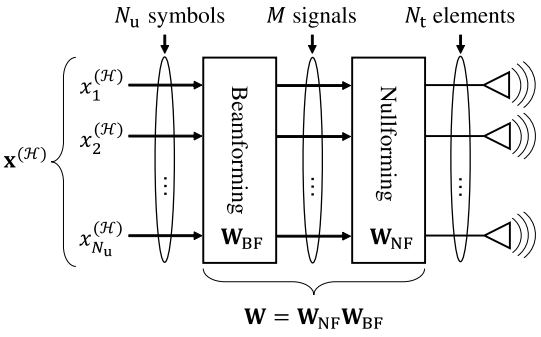

FIGURE 4. Block diagram of the proposed two-stage precoding scheme for massive MU-MIMO systems at the HAPS side.

The overall precoding weight matrix comprises $\mathbf{W}_{\mathrm{NF}}$ and $\mathbf{W}_{\mathrm{BF}}$, and M is the parameter to control their size. Considering the number of nulls formed by $\mathbf{W}_{\mathrm{NF}}$ and $\mathbf{W}_{\mathrm{BF}}$, M can be selected from integers in the interval $[N_{\mathrm{u}}, N_{\mathrm{t}}-N_{\mathrm{b}}]$. The selection of M directly affects the communication performance of HAPSs because M corresponds to the remaining number of elements used to generate beams for H-users. When the overall precoding function in Fig. 4 is implemented as a full-digital precoder, $M = N_{\mathrm{t}} - N_{\mathrm{b}}$ should be selected for maximizing the beamforming performance of $\mathbf{W}_{\mathrm{BF}}$. In general, full-digital precoders can produce high beamforming gains. However, their implementation cost and power consumption are extremely high because of multiple radio frequency (RF) chains. In particular, HAPS systems have much stricter power consumption and payload weight than terrestrial BSs. Thus, a hybrid analog-digital precoding scheme can be an effective alternative to reduce both the implementation cost and power consumption [28]. In Fig. 4, it is possible to implement the nullforming function using an analog precoder because $\mathbf{W}_{\mathrm{NF}}$ is applied to the entire frequency band. However, the beamforming function in Fig. 4 should be implemented by a digital precoder because $\mathbf{W}_{\mathrm{BF}}$ is separately calculated for each group of H-users who share the same time-frequency resource. In this case, M can be interpreted as the number of RF chains required in the hybrid precoder design. Therefore, M is an important parameter to balance the system performance along with power consumption and payload weight in the practical implementation of HAPSs.

IV. SIMULATIONS DETAILS

A. COEXISTENCE SIMULATION MODEL

The proposed two-stage precoding scheme described in Section III has been evaluated through computer simulations, and the respective simulation parameters are listed in Table 1. A single HAPS and multiple terrestrial BSs coexist in a circular service area and use the same frequency band whose bandwidth and center frequency are 18 MHz and 2 GHz, respectively. HAPS is located at an altitude of 20 km, and the radius of its service area is 100 km. The cell deployment model in [18] has been used to determine the locations of terrestrial BSs, where they are sparsely and circularly distributed in the service area. As shown in Fig. 5, the candidate location of a terrestrial BS is defined as a radial grid, where they are equally spaced on circles having different radii. Letting N_{c} be the number of circles in the grid, the position of the k-th candidate point on circle $c \in \{1, \cdots, N_{\mathrm{c}}\}$, denoted by $(x_{c,k}, y_{c,k})$, is given by

$$(x_{c,k}, y_{c,k}) = (cD\cos\phi_{c,k}, cD\ \sin\phi_{c,k}), \tag{29}$$

where D represents the minimum distance between candidate points on different circles, and $\phi_{c,k}$ represents the azimuth angle of the k-th candidate point on circle c. Fig. 5 shows the

TABLE 1. Simulation parameters.

Common	Bandwidth B	18 MHz
	Carrier frequency	2 GHz
HAPS	Number of HAPSs	1
	Altitude of an aircraft	20 km
	Service area radius $R^{(\mathrm{H})}$	100 km
	Total transmit power $P_{\mathrm{t}}^{(\mathcal{H})}$	120 W
	Number of users N_{u}	6, 12, 18, 24, 36, 42
	Array antenna structure	Table 2 and Fig. 7
	Number of elements N_{t}	100, 144, 196, 256
	Radiation pattern of a single antenna element: $\beta_{\mathrm{e}}(\theta,\phi) = 10^{A(\theta,\phi)/20}$	$G_{\max} = 8$ dBi, $\theta_{\mathrm{tilt}} = 0°$, $\theta_{3\mathrm{dB}} = 65°$, $\phi_{3\mathrm{dB}} = 65°$, $SLA_V = 30$ dB, $A_{\max} = 30$ dB
Terrestrial BSs	Number of BSs N_{b}	10, 20, 30, 40, 50
	Number of sectors N_{a}	3 per cell
	Antenna height	50 m
	Cell radius $R^{(\mathrm{G})}$	2 km
	Transmit power $p_s^{(\mathcal{G})}$	20 W per sector
	Radiation pattern of a single sector antenna: $\beta_{\mathrm{s}}(\theta,\phi) = 10^{A(\theta,\phi)/20}$	$G_{\max} = 14$ dBi, $\theta_{\mathrm{tilt}} = 1.15°$, $\theta_{3\mathrm{dB}} = 10°$, $\phi_{3\mathrm{dB}} = 70°$, $SLA_V = 25$ dB, $A_{\max} = 20$ dB
H-users G-users	Number of antennas	1
	Antenna height	1 m
	Antenna gain	-3 dBi
	Radiation pattern	Omnidirectional
	Noise power density	-174 dBm/Hz
	Noise figure	5 dB

radial grid with $N_{\mathrm{c}} = 4$, $D = 20$ km, and $\phi_{c,k} = 60k/c - 90$ degrees, which has 61 candidate points, including the additional point at $(0, 0)$. Finally, the distribution of terrestrial BSs is determined by randomly selecting N_{b} candidates from the grid.

The radius of each terrestrial cell is defined as 2 km, and G-users are located in a terrestrial cell. H-users are located outside the terrestrial cells but inside the HAPS service area. Each H-user and G-user has a single omnidirectional antenna with a gain of -3 dBi, and its height is 1 m.

B. SIMULATION FLOW AND EVALUATION

Fig. 6 shows the flowchart of a simulation for given $N_{\mathrm{u}} \in \{6, 12, 18, 24, 36, 42\}$, $N_{\mathrm{b}} \in \{10, 20, 30, 40, 50\}$, and $N_{\mathrm{t}} \in \{100, 144, 196, 256\}$. First, the locations of N_{b} terrestrial BSs have been determined, and same deployment has been used throughout the simulation with 50 trials. $100 \times N_{\mathrm{u}}$ H-users for each trial have been uniformly and randomly distributed in the service area with a radius of 100 km. Note that they are distributed outside the terrestrial cells. Moreover, 100 G-users have been uniformly and randomly distributed in each sector of all terrestrial BSs. Therefore, each trial has a total of $100 \times N_{\mathrm{a}}N_{\mathrm{b}}$ G-users. To improve the HAPS system capacity, angle-based user selection (AUS) [29] has been applied to create 100 groups of N_{u} H-users with low spatial correlations. $N_{\mathrm{a}}N_{\mathrm{b}}$ G-users from different sectors have been randomly selected

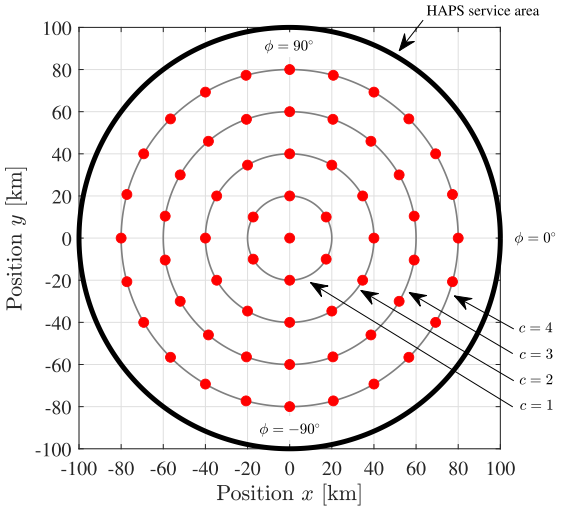

FIGURE 5. Radial grid for the candidate locations of terrestrial BSs in the HAPS service area, with $N_{\mathrm{c}} = 4$, $D = 20$ km, and $\phi_{c,k} = 60k/c - 90$ degrees. Each red dot shows the candidate position of a terrestrial BS, and the HAPS is located at (0, 0).

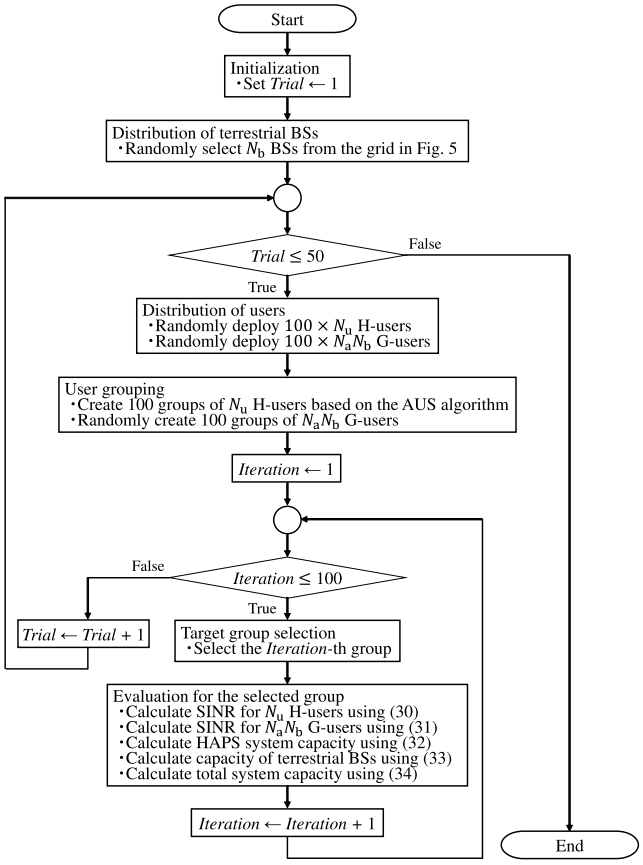

FIGURE 6. Simulation flow for given N_{u}, N_{b}, and N_{t}.

as one group. This process is repeated 100 times to obtain all the 100 groups.

Each trial comprises 100 iterations, where the HAPS and N_{b} terrestrial BSs share a single common frequency band to communicate with N_{u} H-users and $N_{\mathrm{a}}N_{\mathrm{b}}$ G-users in one of the 100 groups in each iteration. To simplify the simulation

model, the HAPS and all terrestrial BSs use only one frequency resource in each iteration; i.e., the entire bandwidth of 18 MHz is used as a single frequency resource, and only N_{u} H-users and N_{a} G-users per cell can be served using the entire frequency band in the simulations. Note that the bandwidth is divided into multiple small frequency resources to accommodate even more users at once in practical communication systems.

This study uses the SINR per user and system capacity as performance indicators. The SINR of H-user u and G-user s in a certain group or iteration, denoted by $\gamma_u^{(\mathrm{H})}$ and $\gamma_s^{(\mathrm{G})}$, can be derived from (3) and (4) as follows:

$$\gamma_u^{(\mathrm{H})} = \frac{\overbrace{\left|\mathbf{h}_u^{(\mathcal{H})}\mathbf{w}_u\right|^2 p_u^{(\mathcal{H})}}^{\text{desired signal}}}{P_{\mathrm{n}} + \underbrace{\sum_{i=1,i\neq u}^{N_{\mathrm{u}}} \left|\mathbf{h}_u^{(\mathcal{H})}\mathbf{w}_i\right|^2 p_i^{(\mathcal{H})}}_{\text{IUI}} + \underbrace{\sum_{j=1}^{N_{\mathrm{a}}N_{\mathrm{b}}} \left|g_{u,j}^{(\mathcal{H})}\right|^2 p_j^{(\mathcal{G})}}_{\text{interference from all BSs}}}, \tag{30}$$

$$\gamma_s^{(\mathrm{G})} = \frac{\overbrace{\left|g_{s,s}^{(\mathcal{G})}\right|^2 p_s^{(\mathcal{G})}}^{\text{desired signal}}}{P_{\mathrm{n}} + \underbrace{\sum_{j=1,j\neq s}^{N_{\mathrm{a}}N_{\mathrm{b}}} \left|g_{s,j}^{(\mathcal{G})}\right|^2 p_j^{(\mathcal{G})}}_{\text{inter-cell interference}} + \underbrace{\sum_{i=1}^{N_{\mathrm{u}}} \left|\mathbf{h}_s^{(\mathcal{G})}\mathbf{w}_i\right|^2 p_i^{(\mathcal{H})}}_{\text{interference from HAPS}}}. \tag{31}$$

Note that (30) includes interference from all N_{b} terrestrial BSs, and (31) includes that from HAPS to properly evaluate the system performances of coexisting HAPS and terrestrial BSs. The HAPS system capacity for a certain iteration is defined as the sum capacity of all N_{u} H-users in the group:

$$C^{(\mathrm{H})} = \sum_{u=1}^{N_{\mathrm{u}}} B\log_2\left(1+\gamma_u^{(\mathrm{H})}\right), \tag{32}$$

where B denotes the system bandwidth. Similarly, the system capacity of terrestrial BSs for a certain iteration is defined as the sum capacity of all $N_{\mathrm{a}}N_{\mathrm{b}}$ G-users in the group:

$$C^{(\mathrm{G})} = \sum_{s=1}^{N_{\mathrm{a}}N_{\mathrm{b}}} B\log_2\left(1+\gamma_s^{(\mathrm{G})}\right). \tag{33}$$

Finally, the total system capacity for a certain iteration can be defined as the sum capacity of the HAPS and terrestrial BSs:

$$C^{(\mathrm{Total})} = C^{(\mathrm{H})} + C^{(\mathrm{G})}. \tag{34}$$

Throughout the 50 simulation trials, we obtain $50\times 100\times N_{\mathrm{u}}$ values of $\gamma_u^{(\mathrm{H})}$, $50\times 100\times N_{\mathrm{a}}N_{\mathrm{b}}$ values of $\gamma_s^{(\mathrm{G})}$, and 50×100 values of $C^{(\mathrm{H})}$, $C^{(\mathrm{G})}$, and $C^{(\mathrm{Total})}$.

C. CONFIGURATION: HAPS

To cover the extremely wide service area having a radius of 100 km with a single aircraft, a cylindrical array antenna has been mounted at the bottom of the aircraft. It comprises N_{h} elements circularly placed in horizontal direction with a spacing of 0.6λ, N_{v} elements linearly arranged in vertical direction with a spacing of 0.5λ, and N_{z} elements at the bottom to cover the area just below the aircraft ($\lambda \approx 15$ cm). The bottom N_{z} elements are uniformly placed on the circle with a radius of $0.6\lambda N_{\mathrm{h}}/(2\pi)$. Hence, the total number of elements is $N_{\mathrm{t}} = N_{\mathrm{h}}N_{\mathrm{v}} + N_{\mathrm{z}}$. Table 2 lists the configuration parameters of four different cylindrical array antennas. Fig. 7 shows the 196-element cylindrical array antenna with $N_{\mathrm{h}} = 31$, $N_{\mathrm{v}} = 6$, and $N_{\mathrm{z}} = 10$. Because of multiple elements deployed on the curved surface, the cylindrical array antenna can cover the entire area having a radius of 100 km. Please refer to [9] for more details on the cylindrical array antenna designed for HAPS service links. The following 3D beam pattern model, which is defined in [30], has been used as the radiation power pattern of each element:

$$A_{\mathrm{V}}(\theta) = \min\left(12\left(\frac{\theta-\theta_{\mathrm{tilt}}}{\theta_{3\mathrm{dB}}}\right)^2, SLA_V\right), \tag{35}$$

$$A_{\mathrm{H}}(\phi) = \min\left(12\left(\frac{\phi}{\phi_{3\mathrm{dB}}}\right)^2, A_{\max}\right), \tag{36}$$

$$A(\theta,\phi) = G_{\max} - \min\left(-\left(A_{\mathrm{V}}(\theta)+A_{\mathrm{H}}(\phi)\right), A_{\max}\right), \tag{37}$$

where $A_{\mathrm{V}}(\theta)$ and $A_{\mathrm{H}}(\phi)$ are the vertical and horizontal cuts of radiation power pattern in dB, respectively. $A(\theta,\phi)$ is the combined 3D radiation power pattern in dBi, with $\theta \in [-90°, 90°]$ and $\phi \in [-180°, 180°]$ being the elevation and azimuth angles, respectively. In (35), θ_{tilt} is the vertical

TABLE 2. Configuration parameters of cylindrical array antennas.

N_{t}	100 (10^2)	144 (12^2)	196 (14^2)	256 (16^2)
N_{h}	23	27	31	35
N_{v}	4	5	6	7
N_{z}	8	9	10	11

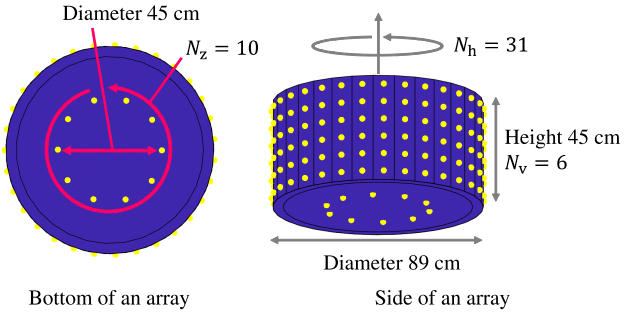

FIGURE 7. Cylindrical array antenna with 196 elements ($N_{\mathrm{h}} = 31$, $N_{\mathrm{v}} = 6$, and $N_{\mathrm{z}} = 10$). This array antenna has $N_{\mathrm{h}}N_{\mathrm{v}} = 186$ and $N_{\mathrm{z}} = 10$ elements on its curved surface and bottom, respectively.

steering angle, $\theta_{3\text{dB}}$ is the vertical 3 dB-beamwidth, and SLA_V is the vertical side-lobe attenuation in dB. In (36), $\phi_{3\text{dB}}$ is the horizontal 3 dB-beamwidth, and $A_{\max}$ is the maximum attenuation in dB. In (37), $G_{\max}$ is the maximum directional gain in dBi. Using this model, the radiation pattern of each element in (15) can be defined as $\beta_{\text{e}}(\theta, \phi) = 10^{A(\theta,\phi)/20}$ with the following configuration parameters: $\theta_{3\text{dB}} = \phi_{3\text{dB}} = 65°$, $\theta_{\text{tilt}} = 0°$, $SLA_V = A_{\max} = 30$ dB, and $G_{\max} = 8$ dBi.

For evaluation, this study compares the results obtained using the conventional MMSE precoder without nullforming, described in (13), with those obtained using the proposed two-stage precoders, presented in (23) and (24). For compact notation, the proposed two-stage precoders based on ZF and MMSE have been referred to as "NF-ZF" and "NF-MMSE," respectively. The total transmit power of the HAPS is 120 W, which is evenly distributed between N_{u} H-users; i.e., $p_u^{(\mathcal{H})} = 120/N_{\text{u}}$ for all $u \in \mathcal{H}$.

D. CONFIGURATION: TERRESTRIAL BASE STATIONS

Assuming a typical three-sector cell, every terrestrial BS has three sector antennas, and their heights equate to 50 m. The transmit power per sector is 20 W; i.e., $p_s^{(\mathcal{G})} = 20$ for all $s \in \mathcal{G}$. The 3D beam pattern model given in (35)–(37) has been used as the radiation power pattern of each sector antenna. The radiation pattern of a single sector antenna in (18) is defined as $\beta_{\text{s}}(\theta, \phi) = 10^{A(\theta,\phi)/20}$ with the following configuration parameters: $\theta_{3\text{dB}} = 10°$, $\theta_{\text{tilt}} = 1.15°$, $\phi_{3\text{dB}} = 70°$, $SLA_V = 25$ dB, $A_{\max} = 20$ dB, and $G_{\max} = 14$ dBi. The above-mentioned parameters are commonly used to evaluate macro-cells [31], [32]. Note that the vertical tilt of 1.15° has been determined to steer the main beam in the direction of the cell boundary having a radius of 2 km.

V. RESULTS AND DISCUSSION

A. PRELIMINARY EVALUATION

First, we start with the performance comparison of the following two nullforming strategies in the first stage:

Case (a): Nulls are directed toward G-users (Fig. 3(a)).
Case (b): Nulls are formed toward BSs (Fig. 3(b)).

The nullforming weight matrix for Case (a) can be obtained by extending $\mathbf{H}^{(\mathcal{B})}$ in (21) and (22) to include all $N_{\text{a}}N_{\text{b}}$ G-users. The nullforming weight matrix for Case (b) is directly calculated using (22). In both cases, ZF has been used in the second stage. Note that "TX-off" shows the case where the HAPS is out of service; i.e., $p_u^{(\mathcal{H})} = 0$ for all $u \in \mathcal{H}$.

Fig. 8 compares the cumulative distribution curves of SINR per user for the above two cases with $N_{\text{u}} = 6, 36$, $N_{\text{b}} = 10$, and $N_{\text{t}} = 196$. Fig. 8(a) shows that the SINR curves of G-users for Case (a) are almost the same as those of TX-off because Case (a) minimizes the interference from HAPS to G-users. The important point is that the difference in the SINR of G-users between Cases (a) and (b) is only around 1–1.2 dB. Unlike similar curves in Fig. 8(a), the SINR curves of H-users differ in the two cases. In Fig. 8(b), the median (50th percentile) of the SINR values for Case (b) is larger than

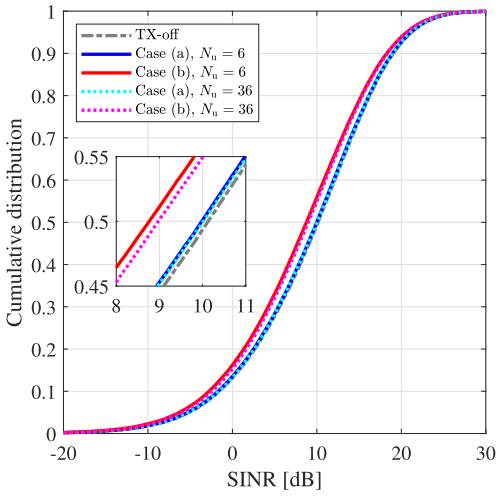

(a) G-users

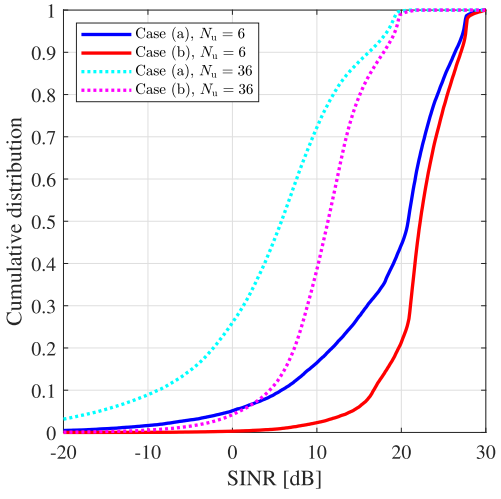

(b) H-users

FIGURE 8. Cumulative distribution curves of the SINR per user for Cases (a) and (b) with $N_{\text{u}} = 6, 36$, $N_{\text{b}} = 10$, and $N_{\text{t}} = 196$. In both cases, ZF is used in the second stage.

that of Case (a) by about 1.4 dB with $N_{\text{u}} = 6$ and 5.7 dB with $N_{\text{u}} = 36$, which is attributed to the difference in the remaining number of antenna elements or degrees of freedom of an array antenna after the nullforming process. Case (a) forms $N_{\text{a}}N_{\text{b}}$ nulls in the first stage, whereas Case (b) creates only N_{b} nulls. Case (b) can generate higher-gain beams for H-users than Case (a) because the remaining number of elements used in the second stage is $196 - 3 \times 10 = 166$ for Case (a) and $196 - 10 = 186$ for Case (b).

Fig. 9 compares the cumulative distribution curves of the system capacities for Cases (a) and (b) with $N_{\text{u}} = 6, 36$, $N_{\text{b}} = 10$, and $N_{\text{t}} = 196$. Similar to the distribution curves in Fig. 8, Case (a) outperforms Case (b) considering the terrestrial capacity in Fig. 9(a), whereas Case (b) shows better HAPS capacities than Case (a). Consequently, for $N_{\text{u}} = 6$ in Fig. 9(c), no large difference can be recognized in the total capacity curves of Cases (a) and (b). However, for

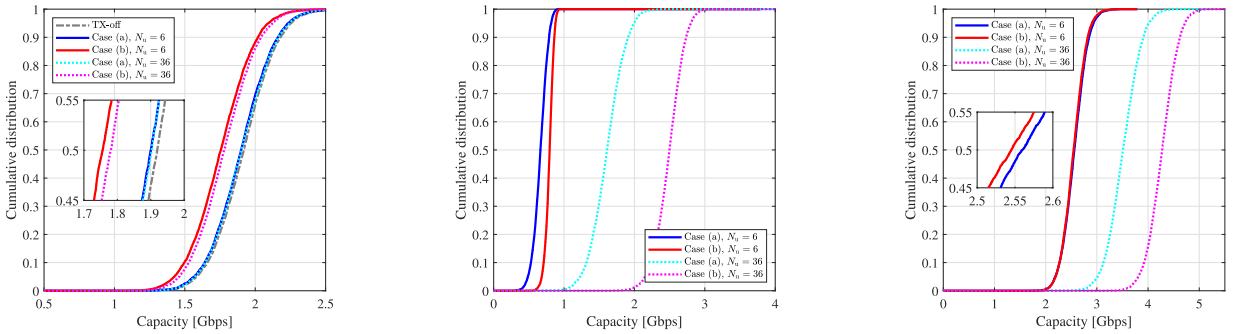

(a) Terrestrial BSs (b) HAPS (c) Total

FIGURE 9. Cumulative distribution curves of the system capacities for Cases (a) and (b) with $N_u = 6, 36$, $N_b = 10$, and $N_t = 196$. In both cases, ZF is used in the second stage.

$N_u = 36$, the total capacity for Case (b) greatly exceeds that of Case (a). Finally, the results in Fig. 9(c) demonstrate that Case (b) shows similar performance to Case (a) with small N_u and an even better total capacity than Case (a) with large N_u.

Considering the above preliminary evaluation results and the serious drawback of Case (a) described in Section III-B, the proposed two-stage precoding scheme adopts Case (b) as a nullforming policy in the first stage. Note that the results of the proposed precoders in the following Sections V-B to V-E are obtained using Case (b).

B. FUNDAMENTAL EVALUATION

This section describes the basic evaluation results of the proposed two-stage precoding scheme with $N_u = 36$, $N_b = 10$, and $N_t = 196$. Fig. 10 shows the cumulative distribution curves of the SINR per user with $N_u = 36$, $N_b = 10$, and $N_t = 196$. The following two different values of M have been used in the proposed precoders: $M = 186$ is the maximum value for $N_b = 10$, and $M = 93$ reduces the number of elements used to form user-specific beams by half.

Comparing the distribution curves in Figs. 10(a) and 10(b), the precoder that achieves higher SINR values in Fig. 10(b) tends to show lower SINR values in Fig. 10(a). Higher-gain beams formed by the cylindrical array antenna are beneficial for H-users to improve their SINR. However, they strongly interfere with G-users. Specifically, the conventional MMSE performs best considering the SINR of H-users. Moreover, it also shows the worst performance considering the SINR of G-users because of its strong interference. In Fig. 10(a), the median of the SINR values of the conventional MMSE is only about 0.1 dB, whereas that of TX-off is around 10.2 dB. Alternatively, the SINR of G-users reduces by over 10 dB when the HAPS uses the conventional MMSE precoder. However, no large degradation can be recognized in the SINR curves of the proposed precoders in Fig. 10(a). The proposed precoders suppress the interference from the HAPS to G-users. Hence, they achieve 8.9 dB as the median of SINR values of G-users in Fig. 10(a). In exchange for this nullforming-based interference mitigation, the SINR of H-users decreases when the proposed precoders are used, compared to the conventional

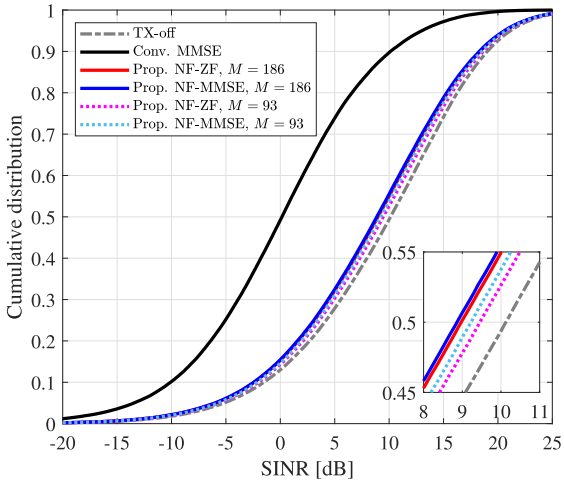

(a) G-users

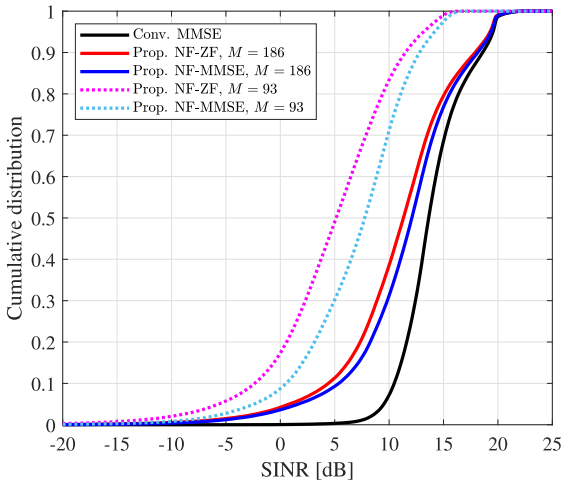

(b) H-users

FIGURE 10. Cumulative distribution curves of the SINR per user for the case of $N_u = 36$, $N_b = 10$, and $N_t = 196$.

MMSE. The proposed precoders with $M = 186$ outperform those with $M = 93$ in Fig. 10(b). As explained previously, M is the number of antenna elements used to create user-specific

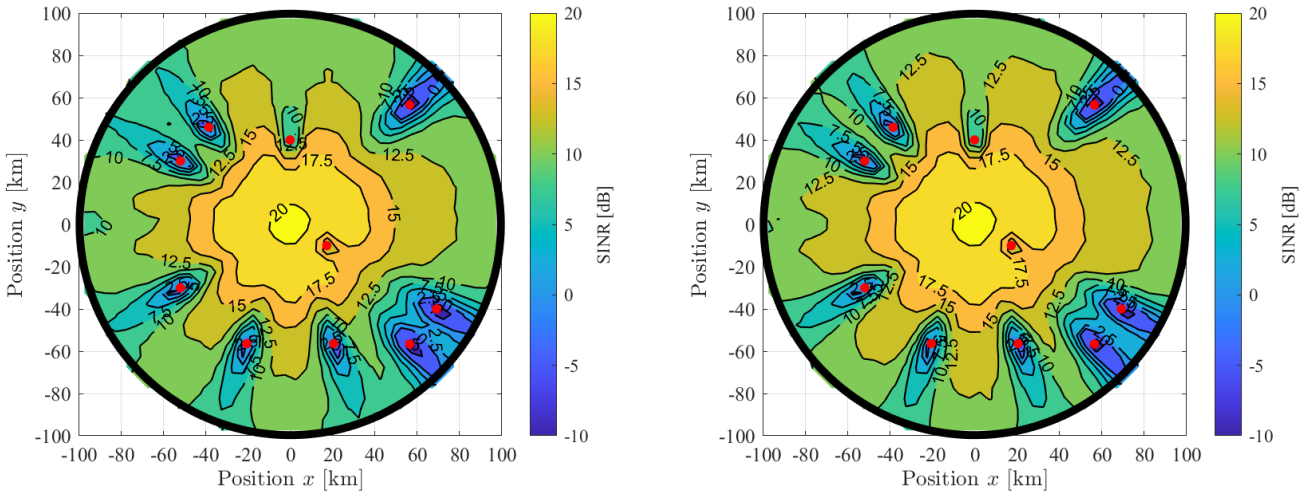

(a) Prop. NF-ZF with $M = 186$

(b) Prop. NF-MMSE with $M = 186$

FIGURE 11. SINR heatmaps of H-users in the HAPS service area with a radius of 100 km for the case of $N_u = 36$, $N_b = 10$, and $N_t = 196$. The HAPS is located at (0, 0). Each red dot shows the location of a terrestrial BS.

beams; thus, the SINR of H-users increases in proportion to M. Fig. 10(a) confirms that the proposed precoders can successfully mitigate the interference from the HAPS to G-users, regardless of M.

Fig. 11 presents the SINR heatmaps of H-users obtained using the proposed precoders at $N_u = 36$, $N_b = 10$, and $N_t = 196$. These heatmaps are created by dividing the service area into multiple 5 km $\times$ 5 km grids and calculating the average SINR for each square grid. Each red dot in Fig. 11 shows the location of a terrestrial BS, and the HAPS is located at the center of the service area. As an overall trend, the SINR of H-users is considerably high around the center of the service area or the area below the aircraft; it then reduces with increase in the distance between the HAPS and H-users. In Fig. 11, H-users around terrestrial BSs tend to have significantly lower SINR values than others, which is caused by the nullforming in the proposed precoders and the interference from terrestrial cells. This shows that the proposed precoders successfully create the ten nulls targeting the ten terrestrial BSs. Comparing the heatmaps in Figs. 11(a) and 11(b), NF-MMSE outperforms NF-ZF in the SINR of H-users over the entire service area, and it achieves higher SINR values in a wider area than NF-ZF; e.g., the area with an SINR of over 12.5 dB accounts for about 35% in Fig. 11(a) and 43% in Fig. 11(b).

Fig. 12 shows the SINR heatmaps of G-users in the terrestrial cell located around (56.6, 56.6) in km in Fig. 11. They are created by dividing the cell into 100 m $\times$ 100 m grids and calculating the average SINR for each square grid. Fig. 12(a) shows the SINR heatmap of G-users in the absence of HAPS, where three sector beams cover the circular area of a radius of 2 km. In Fig. 12(b), the SINR of G-users drastically reduces over the entire coverage of the cell when the conventional MMSE is used. The area with an SINR of less than 0 dB accounts for around 35% in Fig. 12(b). In contrast, the SINR heatmaps of the proposed precoders in Figs. 12(c) and 12(d) are almost equivalent to that in Fig. 12(a). As illustrated in Fig. 3, the proposed precoders create a single pinpoint null for each terrestrial cell, targeting the elevation and azimuth angles corresponding to the center of the cell. However, the elevation and azimuth angles of G-users in a terrestrial cell are slightly different from those of the center of the cell. The center of the terrestrial cell in Fig. 12 is located at an azimuth $\phi = 45°$, and the cell radius is 2 km. In this case, the azimuth angle of G-users in the cell is in the range of $45° \pm 1.5°$. In particular, G-users around cell boundaries are apart from the direction of the null by several degrees, which results in the remaining interference from the HAPS to these G-users. Because of the residual interference, the SINR around the cell boundaries in Figs. 12(c) and 12(d) is slightly lower than that in Fig. 12(a). The proposed precoders can significantly reduce the HAPS interference to G-users. However, it is difficult to completely remove the interference to cell-edge users.

Fig. 13 shows the deployment of H-users for plotting the radiation power patterns in Fig. 14. To capture multiple nulls and user-specific beams simultaneously, six H-users, users 1 to 6, are arranged at regular intervals on the circle with a radius of 60 km. In Fig. 13, blue cross marks indicate their location. Their azimuth angles are $-112.5°$, $-103.5°$, $-94.5°$, $-85.5°$, $-76.5°$, and $-67.5°$, where the angular difference between two adjacent H-users is only 9°. In Fig. 14, a dashed vertical line represents the azimuth angle of an H-user, and a red solid line plots that of a terrestrial BS. As the aircraft is at an altitude of 20 km, the direction from the array antenna to the circle with a radius of 60 km corresponds to the elevation angle of about 18.4°.

Fig. 14 shows the exemplification of beam patterns for the case of $N_u = 36$, $N_b = 10$, and $N_t = 196$, which is the azimuth cut of radiation power patterns of the cylindrical

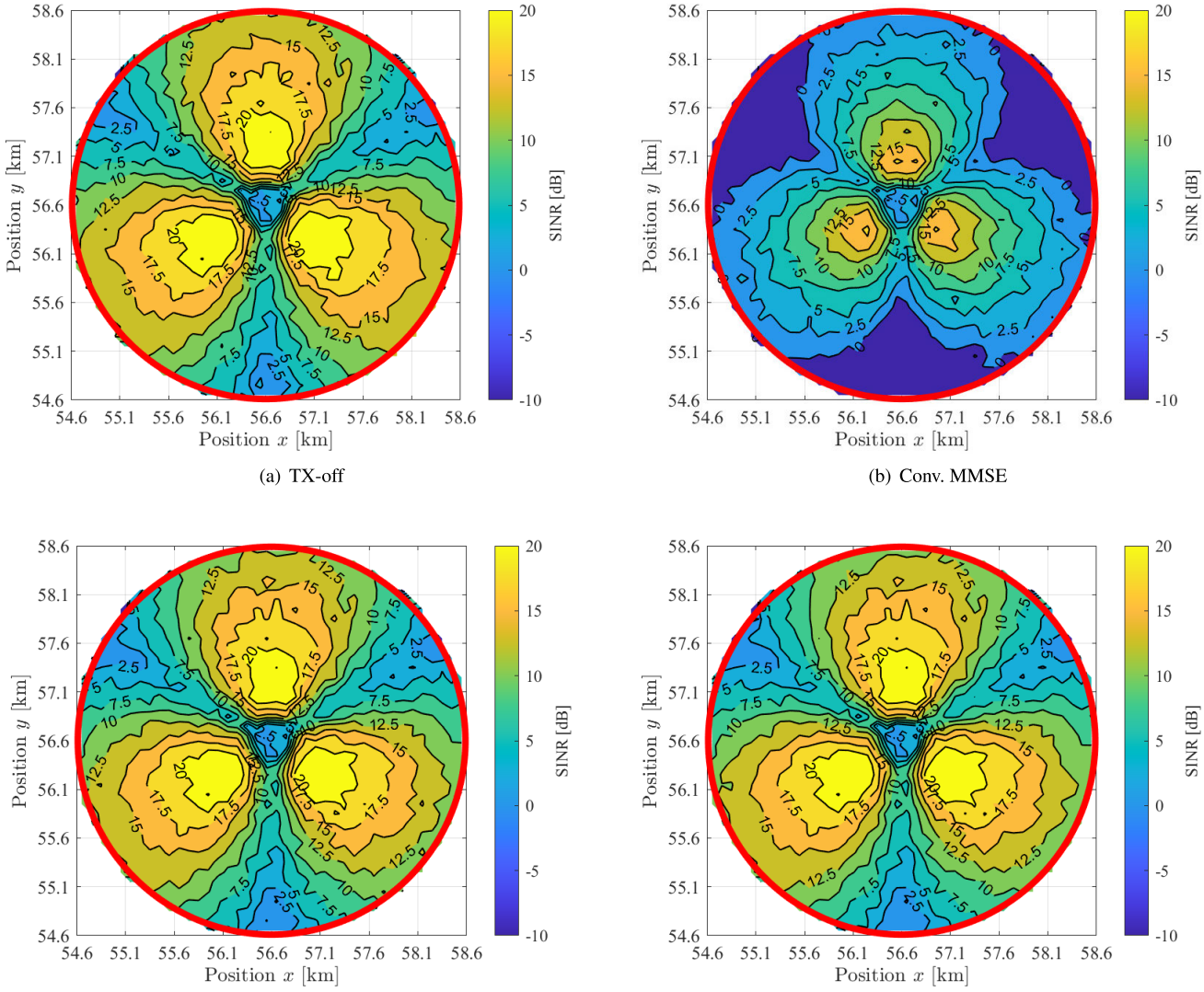

(a) TX-off

(b) Conv. MMSE

(c) Prop. NF-ZF with $M = 186$

(d) Prop. NF-MMSE with $M = 186$

FIGURE 12. SINR heatmaps of G-users in a terrestrial cell with a radius of 2 km for the case of $N_u = 36$, $N_b = 10$, and $N_t = 196$, where the terrestrial BS is located around (56.6, 56.6) in km in Fig. 11.

array antenna with the proposed precoders. Focusing on the two red solid lines in both Figs. 14(a) and 14(b), the beam gains for all six H-users considerably decrease at both $\phi = -110°$ and $-70°$, which are nulls formed in directions of BSs 1 and 2 in Fig. 13. Because of these nulls, the proposed precoders can prevent signals transmitted to H-users from interfering with terrestrial cells. When a terrestrial BS and H-user are located close to each other, their spatial correlation becomes higher. Therefore, gains in directions of users 1 and 6 are lower than those of users 3 and 4 in Figs. 14(a) and 14(b). Even in such a high correlation situation, the proposed precoders are designed to prioritize nullforming for terrestrial BSs; thus, the beam gains around terrestrial cells decrease sharply in both Figs. 14(a) and 14(b). Here, focusing on the difference between Figs. 14(a) and 14(b), the beam gains of NF-MMSE are higher than those of NF-ZF by approximately 1.2–2.7 dB. NF-ZF completely removes the IUI; it creates a total of eight complete null points in Fig. 14(a). However, NF-MMSE increases the beam gains by tolerating the IUI; two complete nulls for BSs 1 and 2 and six imperfect nulls for users 1 to 6 are identified in Fig. 14(b).

C. PERFORMANCE VS. THE NUMBER OF H-USERS

This section compares the proposed precoders with the conventional MMSE in terms of the performance with different numbers of H-users. The simulation with 50 trials in Fig. 6 is separately performed for each $N_u \in \{6, 12, 18, 24, 36, 42\}$ with $N_b = 10$ and $N_t = 196$.

Fig. 15 shows the SINR per user versus the number of H-users curves. In Fig. 15(a), when the HAPS is out of service (TX-off), the SINR of G-users becomes a constant value of

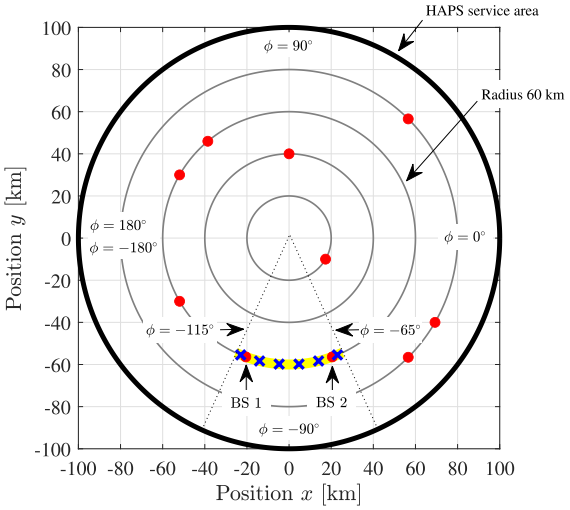

FIGURE 13. Deployment of H-users for capturing the beam patterns in Fig. 14 for the case of $N_u = 36$, $N_b = 10$, and $N_t = 196$. Blue cross marks indicate the location of six H-users, equally spaced on the circle of a radius of 60 km. Their azimuth angles are $\phi = -112.5°, -103.5°, -94.5°, -85.5°, -76.5°$, and $-67.5°$.

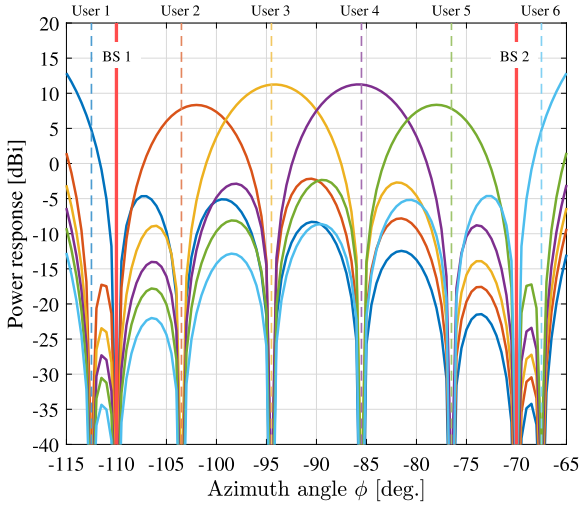

(a) Prop. NF-ZF with $M = 186$

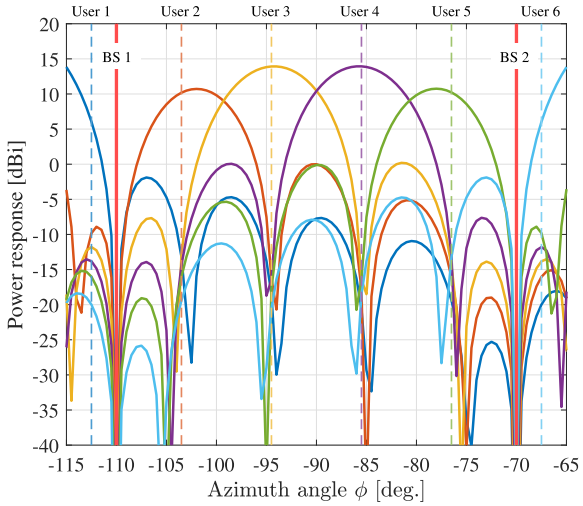

(b) Prop. NF-MMSE with $M = 186$

FIGURE 14. Beam pattern obtained using the proposed precoders at $N_u = 36$, $N_b = 10$, and $N_t = 196$, with the user deployment given in Fig. 13. These figures are the azimuth cut of radiation power patterns of the cylindrical array antenna at the elevation angle of about 18.4°, and their azimuth range corresponds to the yellow arc in Fig. 13. A dashed vertical line represents the azimuth angle of an H-user, and a red solid line plots that of a terrestrial BS.

about 10.2 dB because of no interference from the HAPS. When the proposed precoders are used, the SINR of G-users becomes relatively high for all N_u owing to the nullforming; however, it is lower than 10.2 dB by up to 1.5 dB. This degradation is primarily attributed to the residual interference from the HAPS to G-users located away from the center of a cell, as explained in the previous section. In contrast, the conventional MMSE shows even lower SINR values than the proposed precoders because of its strong interference.

As an overall tread in Fig. 15(b), the SINR of H-users decreases with every precoding scheme for the following reasons. First, the total transmit power is uniformly allocated to H-users; the power per H-user reduces with increase in N_u. In addition, the condition number of $\mathbf{H}^{(\mathcal{H})}$ becomes larger with increase in N_u. Alternatively, $\mathbf{H}^{(\mathcal{H})}$ tends to become ill-conditioned with large N_u because it is more difficult in user grouping to select N_u H-users with better spatial separation or lower spatial correlation when N_u becomes larger. Consequently, both the reduction in transmit power per H-user and increase in condition number of $\mathbf{H}^{(\mathcal{H})}$ lead to a decrease in the received signal power, which results in monotonically decreasing SINR curves of H-users in Fig. 15(b). In contrast, as shown in Fig. 15(a), the SINR values of G-users with the proposed precoders rise gradually with increase in N_u because of the reduction in interference power from the HAPS. The conventional MMSE demonstrates the best SINR performance in Fig. 15(b) as it produces higher-gain beams than the proposed precoders by exploiting all $196 - 1 = 195$ degrees of freedom of the cylindrical array antenna. On the other hand, the proposed precoders require ten degrees of freedom for the nullforming toward ten terrestrial BSs. The number of degrees of freedom used for creating user-specific beams is $186 - 1 = 185$ with $M = 186$ and $93 - 1 = 92$ with $M = 93$. Hence, the precoders with larger M show higher SINR values of H-users in Fig. 15(b). Comparing NF-ZF with NF-MMSE in Fig. 15(b), the SINR values of NF-ZF are almost equivalent to those of NF-MMSE when N_u is smaller than 24 with $M = 186$ and 18 with $M = 93$. This is because both ZF and MMSE precoders are equivalent in the asymptotically high signal-to-noise ratio (SNR) regime [33]. As N_u approaches zero, (24) becomes (23) because the regularization factor in (24) forms a zero matrix. In the low SNR regime or when N_u is large, NF-MMSE shows higher SINR values than NF-ZF in Fig. 15(b). As explained previously, the condition number of $\mathbf{H}^{(\mathcal{H})}$ or $\tilde{\mathbf{H}}^{(\mathcal{H})}$ increases in proportion to N_u. The regularization factor in NF-MMSE can avoid the inversion of such an ill-conditioned matrix. Therefore,

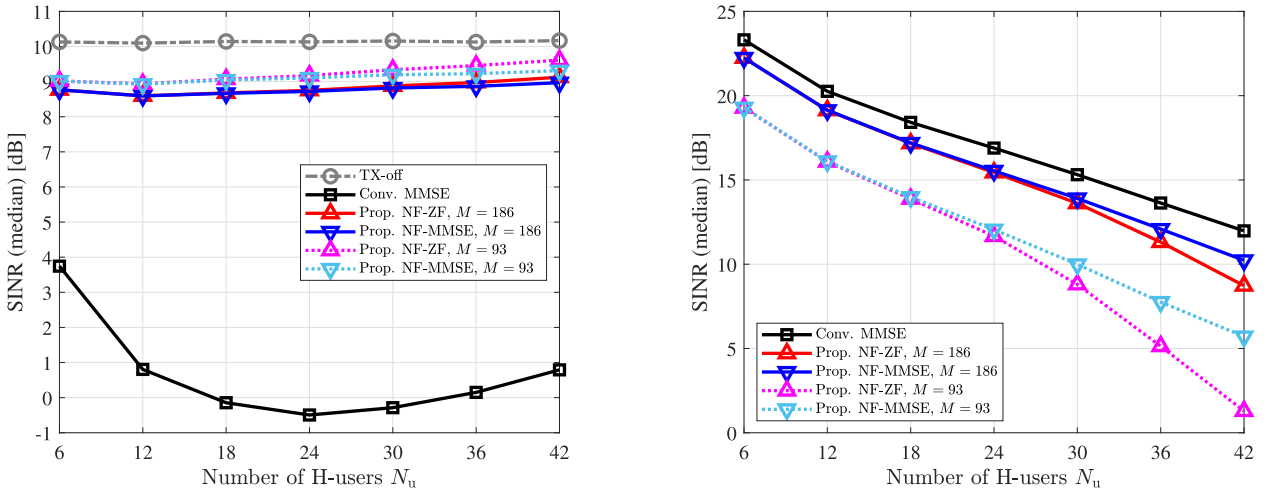

(a) G-users (b) H-users

FIGURE 15. SINR per user versus the number of H-users curves for $N_u \in \{6, 12, 18, 24, 36, 42\}$ with $N_b = 10$ and $N_t = 196$.

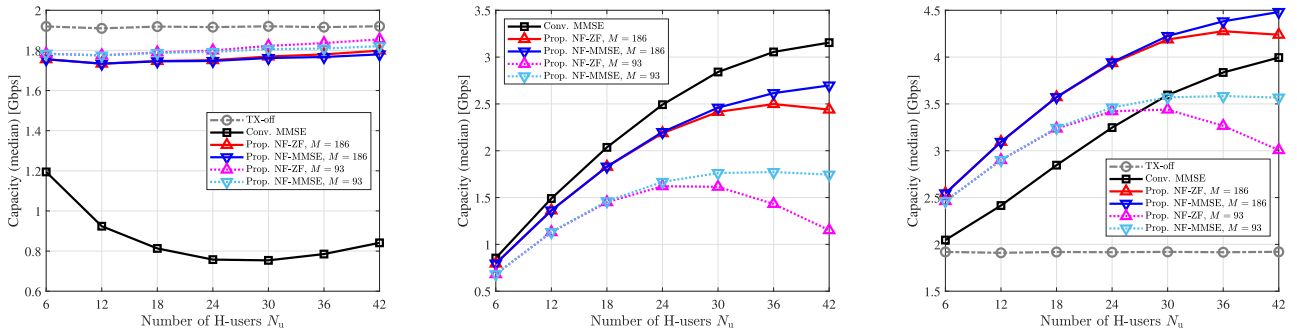

(a) Terrestrial BSs (b) HAPS (c) Total

FIGURE 16. System capacity versus the number of H-users curves for $N_u \in \{6, 12, 18, 24, 36, 42\}$ with $N_b = 10$ and $N_t = 196$.

NF-MMSE shows better SINR values of H-users than NF-ZF in Fig. 15(b).

Fig. 16 shows the system capacity versus the number of H-users curves, where the capacity values have been calculated based on (32)–(34). The terrestrial capacity curves in Fig. 16(a) are similar to G-users' SINR curves in Fig. 15(a). The terrestrial capacity reaches 1.91 Gbps when the HAPS is out of service. Owing to the interference mitigation, the proposed precoders achieve 1.73 Gbps in the terrestrial capacity for all N_u, which corresponds to about 91% of the interference-free case (TX-off). The terrestrial capacity obtained using the conventional MMSE falls below 1 Gbps when N_u is greater than 12 in Fig. 16(a) because of the strong interference.

As described in (32), the HAPS system capacity is defined as the sum capacity of all N_u H-users spatially multiplexed on the same frequency resource in each iteration. In theory, the capacity of MU-MIMO systems with N_u single-antenna users rises in proportion to N_u ($N_u \leq N_t$) [34]. Therefore, the HAPS capacity curves in Fig. 16(b) continue to increase in the small N_u regime. However, the HAPS capacity reaches a peak at a certain N_u. It then decreases because of increase in spatial correlations, which is obvious in the curves of NF-ZF shown in Fig. 16(b). In Fig. 16(b), the HAPS capacity obtained using the conventional MMSE is around 1.48 Gbps at $N_u = 12$ and 3.05 Gbps at $N_u = 36$, whereas that obtained using NF-MMSE with $M = 186$ is greater than 1.36 Gbps at $N_u = 12$ and 2.61 Gbps at $N_u = 36$. Alternatively, NF-MMSE with $M = 186$ achieves 91% and 85% of the HAPS capacity of the conventional MMSE at $N_u = 12$ and $N_u = 36$, respectively. This degradation is primarily attributed to the reduction in the number of degrees of freedom for user-specific beams due to the nullforming.

Figs. 16(a) and 16(b) confirm that the proposed precoders can improve the terrestrial capacity by suppressing the HAPS interference to G-users, whereas they cause the deterioration in the HAPS capacity. Therefore, the total system capacity defined in (34), including the HAPS and all terrestrial BSs, is the most important performance indicator. In Fig. 16(c), the proposed precoders with $M = 186$ outperform the conventional MMSE for all N_u. Specifically, the total capacity achieved by NF-MMSE with $M = 186$ is over 3.09 Gbps at

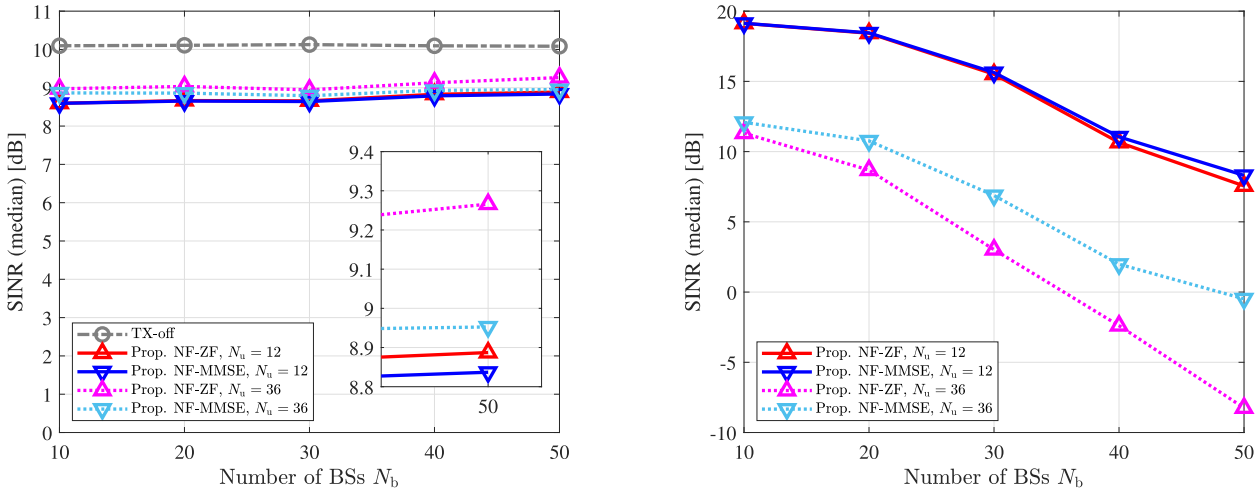

(a) G-users (b) H-users

FIGURE 17. SINR per user versus the number of terrestrial BSs curves for $N_b \in \{10, 20, 30, 40, 50\}$ with $N_u = 12$, 36 and $N_t = 196$. Maximum M is selected in the proposed precoders for each N_b ($M = 196 - N_b$).

$N_u = 12$ and 4.38 Gbps at $N_u = 36$, whereas that achieved by the conventional MMSE is around 2.41 Gbps at $N_u = 12$ and 3.84 Gbps at $N_u = 36$. Alternatively, NF-MMSE with $M = 186$ achieves 128% and 114% of the total capacity of the conventional MMSE at $N_u = 12$ and $N_u = 36$, respectively. The proposed precoders with $M = 93$ are also superior to the conventional MMSE in total capacity when N_u is smaller than 24. In contrast, when N_u becomes larger, the conventional MMSE outperforms the proposed precoders with $M = 93$ in Fig. 16(c). To summarize, for $N_b = 10$, the proposed precoders can improve the total capacity without a lot of reduction in terrestrial capacity if both N_u and M have been properly determined.

D. PERFORMANCE VS. THE NUMBER OF TERRESTRIAL BASE STATIONS

This section focuses on the communication performance of the proposed precoders with respect to different numbers of terrestrial BSs, where the simulation with 50 trials described in Fig. 6 is separately performed for each $N_b \in \{10, 20, 30, 40, 50\}$ with $N_u = 12$, 36 and $N_t = 196$. In addition to the results obtained using the proposed precoders, those of the TX-off case are presented for reference. Maximum M is selected in the proposed precoders for each N_b; i.e., $M = 196 - N_b$. Note that the results of the conventional MMSE without nullforming have been omitted in this section because its performances are independent of N_b.

Fig. 17 shows the SINR per user versus the number of terrestrial BSs curves. In Fig. 17(a), the SINR of G-users obtained using the proposed precoders remains constantly high for all N_b. Among them, NF-MMSE with $N_u = 12$ has the lowest SINR values in Fig. 17(a). Even in this worst case, the SINR achieved by NF-MMSE with $N_u = 12$ is more than 8.64 dB, which is sufficiently high for G-users to communicate with a terrestrial BS. Fig. 17(a) shows that G-users are successfully protected by nulls formed by the proposed precoders even when the number of terrestrial cells increases. In theory, the proposed precoders with N_u H-users can create $N_t - N_u$ nulls for terrestrial BSs; e.g., $196 - 12 = 184$ nulls for terrestrial BSs are allowed in total for the case of $N_u = 12$. However, as shown in Fig. 17(b), many nulls for terrestrial BSs lead to a degradation in the SINR of H-users.

In Fig. 17(b), the proposed precoders demonstrate monotonically decreasing SINR curves of H-users with increase in N_b. The maximum number of degrees of freedom used to create user-specific beams is $N_t - N_b - 1$. In other words, the proposed precoders produce higher-gain beams when N_b is smaller, which results in monotonically decreasing curves in Fig. 17(b). In addition, Fig. 17(b) shows that the difference in SINR values between NF-ZF and NF-MMSE with $N_u = 36$ is larger than those with $N_u = 12$. This is because NF-MMSE works more effectively for a larger number of total nulls or equivalently for channel matrices with a larger condition number. As stated in Section III-D, the theoretical condition, $N_b + N_u \leq N_t$, should be satisfied for successful nullforming and beamforming in the proposed scheme. Even if this condition is fulfilled, the SINR values of H-users fall below 0 dB in certain cases in Fig. 17(b), particularly when N_b becomes large. In practice, the minimum requirement for SINR is specified in communication standards; e.g., the minimum SINR required for LTE service is -6.9 dB [35]. Accordingly, $N_b + N_u$ should be considerably smaller than N_t to satisfy the minimum SINR requirement; i.e., the practical condition is given by $N_b + N_u \ll N_t$.

Fig. 18 shows the system capacity versus the number of terrestrial BSs curves with $N_u = 12$ and 36. In Fig. 18(a), the terrestrial capacity curves obtained using the proposed precoders linearly increase as the number of terrestrial BSs increases. Furthermore, the proposed precoders achieve 91% of the terrestrial capacity of TX-off for all N_b. Similar to

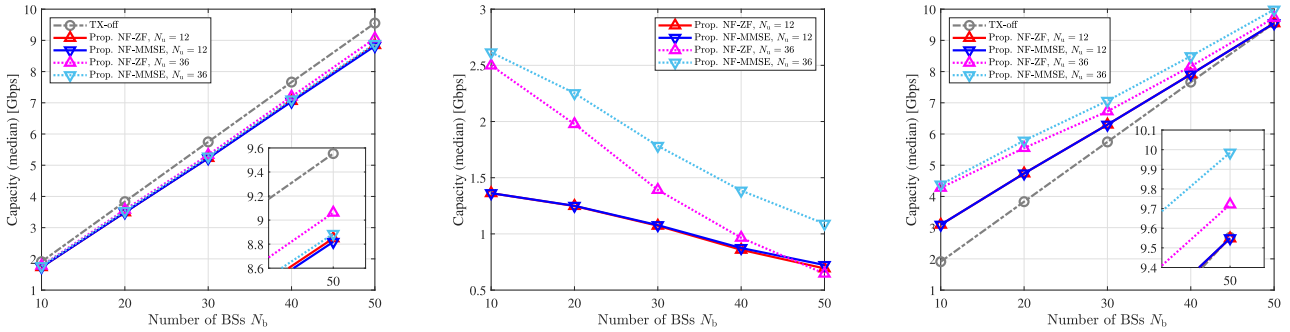

(a) Terrestrial BSs (b) HAPS (c) Total

FIGURE 18. System capacity versus the number of terrestrial BSs curves for $N_b \in \{10, 20, 30, 40, 50\}$ with $N_u = 12$, 36 and $N_t = 196$. Maximum M is selected in the proposed precoders for each N_b ($M = 196 - N_b$).

SINR curves of H-users presented in Fig. 17(b), the HAPS capacity curves obtained using the proposed precoders in Fig. 18(b) monotonically decrease with increase in N_b. This is because the number of spatially multiplexed H-users is fixed to $N_u = 12$ and 36 in Fig. 18(b), unlike the increasing spatially multiplexed H-users in Fig. 16(b). The benefit of spatial multiplexing surpasses the degradation in the SINR or capacity of each H-user when the number of terrestrial BSs is sufficiently small. Thus, the proposed precoders with $N_u = 36$ provide a larger HAPS capacity than those with $N_u = 12$ when N_b is smaller. However, with increase in the number of terrestrial BSs, it becomes difficult to increase the HAPS capacity using the spatial multiplexing technique because of the reduction in SINR per H-user, as shown in Fig. 17(b). Consequently, in Fig. 18(b), NF-ZF with $N_u = 36$ shows a slightly lower HAPS capacity than that with $N_u = 12$ at $N_b = 50$ despite the larger number of spatially multiplexed H-users.

Fig. 18(c) shows that the total capacity curves obtained using the proposed precoders linearly increase with increase in N_b. NF-MMSE with $N_u = 36$ shows the highest total capacity for all N_b, and it achieves 4.38 Gbps at $N_b = 10$ and 9.99 Gbps at $N_b = 50$. Alternatively, it achieves 229% and 105% of TX-off capacities at $N_b = 10$ and 50, respectively. From these results, the proposed precoders improve the total capacity more effectively when N_b is smaller. As explained previously, the terrestrial capacity curves in Fig. 18(a) linearly rise, whereas the HAPS capacity curves in Fig. 18(b) decrease as N_b increases. Therefore, as long as the HAPS capacity in Fig. 18(b) exceeds the degradation in terrestrial capacity in Fig. 18(a), the proposed precoders can achieve a larger total capacity than TX-off in Fig. 18(c). Note that the coverage area of mobile networks is further extended using the HAPS with the proposed precoders even when the total capacity cannot be significantly enhanced with large N_b.

E. PERFORMANCE VS. THE NUMBER OF ANTENNA ELEMENTS

Finally, this section presents the performance of the proposed precoders with respect to different numbers of antenna elements, where the simulation with 50 trials shown in Fig. 6 is separately performed for each $N_t \in \{100, 144, 169, 256\}$ with $N_u = 12$, 36 and $N_b = 10$. In addition to the results obtained using the proposed precoders, those in the case of TX-off are presented for reference. Maximum M is selected for each N_t; i.e., $M = N_t - 10$.

Fig. 19 presents the curves of SINR per user versus the number of antenna elements. As shown in Fig. 19(a), the SINR of G-users becomes constant in the absence of HAPS. The SINR of G-users tends to decrease with increase in N_t when the proposed precoders are used. As N_t increases, the width of a null decreases gradually. Thus, the residual interference from the HAPS to terrestrial cells increases with increase in N_t. In contrast to the decreasing SINR curves in Fig. 19(a), the SINR of H-users in Fig. 19(b) increases monotonically. Regardless of N_u, higher-gain beams are formed toward H-users by an array antenna with larger N_t or equivalently M. In Fig. 19(b), NF-MMSE outperforms NF-ZF with $N_u = 36$, whereas these two precoders show almost the same curves with $N_u = 12$ for all N_t. Please refer to Section V-C for the performance difference between NF-ZF and NF-MMSE with different N_u.

Fig. 20 shows the system capacity versus the number of antenna elements curves with $N_u = 12$ and 36. In Fig. 20(a), the terrestrial capacities of the proposed precoders linearly decrease as the number of antenna elements increases. Owing to the nullforming technique, the proposed precoders achieve 89% of the terrestrial capacity of TX-off even in the worst case with $N_t = 256$ and $N_u = 12$ in Fig. 20(a). Similar to SINR curves of H-users in Fig. 19(b), the HAPS capacities of the proposed precoders in Fig. 20(b) monotonically increase with increase in N_t. Furthermore, the total capacities of the proposed precoders in Fig. 20(c) also monotonically increase with increase in N_t. Because of a larger number of spatially multiplexed H-users, the proposed precoders with $N_u = 36$ offer higher capacity values than those with $N_u = 12$ at almost all N_t in Figs. 20(b) and 20(c). The most important point is that the HAPS capacities in Fig. 20(b) surpass degradation in the terrestrial capacities in Fig. 20(a) for all N_t when the HAPS uses the proposed precoders. Therefore, the proposed scheme improves the total capacity in Fig. 20(c), regardless of the number of antenna elements.

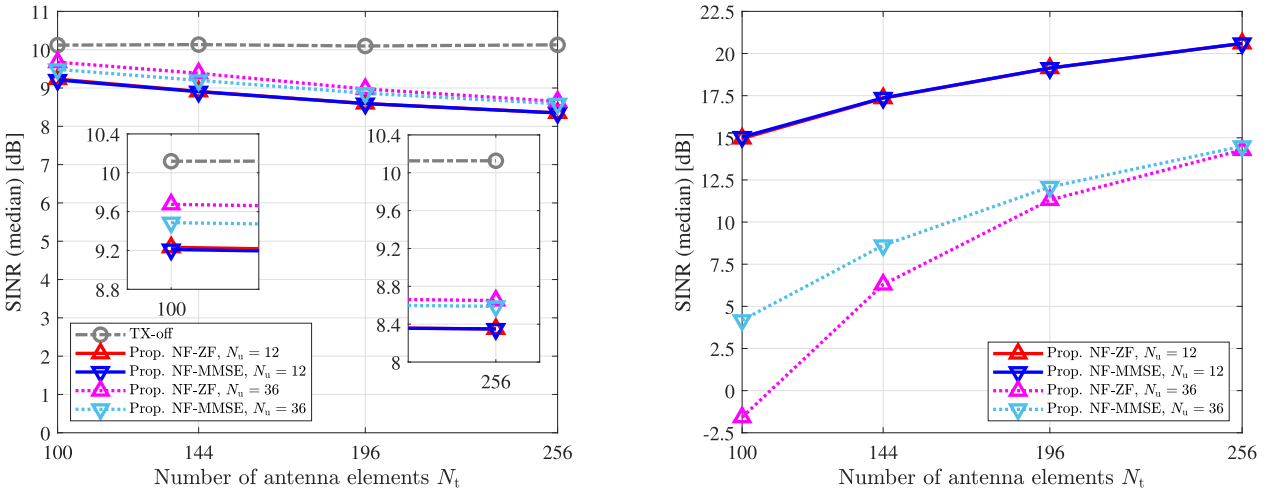

(a) G-users (b) H-users

FIGURE 19. SINR per user versus the number of antenna elements curves for $N_t \in \{100, 144, 196, 256\}$ with $N_u = 12, 36$ and $N_b = 10$. Maximum M is selected in the proposed precoders for each N_t ($M = N_t - 10$).

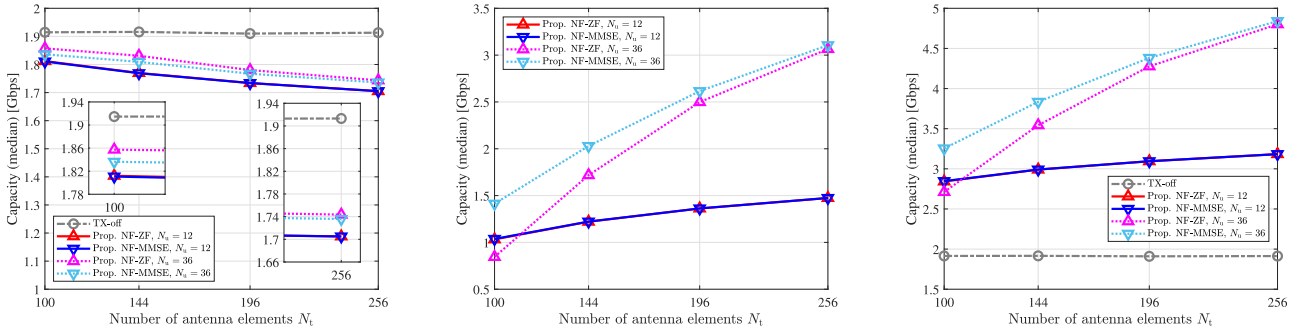

(a) Terrestrial BSs (b) HAPS (c) Total

FIGURE 20. System capacity versus the number of antenna elements curves for $N_t \in \{100, 144, 196, 256\}$ with $N_u = 12, 36$ and $N_b = 10$. Maximum M is selected in the proposed precoders for each N_t ($M = N_t - 10$).

VI. CONCLUSION

This study has proposed a two-stage precoding scheme that realizes spectrum sharing between HAPS and terrestrial BSs. Multiple nulls are formed in the azimuth and elevation angles of terrestrial BSs to mitigate the interference from the HAPS to G-users in the first stage. User-specific beams are formed in directions of H-users in the second stage by exploiting all the remaining degrees of freedom of an array antenna. Because of the precoder design where the nulls and beams are separately controlled, existing precoders for MU-MIMO can be used as beamformers in the second stage. For $N_t = 196$, the results demonstrate that the terrestrial capacity achieved with the proposed precoders is more than 91% of the terrestrial capacity in the case where the HAPS is out of service, regardless of the number of spatially multiplexed H-users and terrestrial BSs. Moreover, the proposed precoders achieve a larger total capacity than the conventional MMSE when the number of total nulls to be created is sufficiently smaller than that of antenna elements. Hence, the proposed scheme realizes spectrum sharing between the HAPS and terrestrial BSs under the condition of $N_b + N_u \ll N_t$. The coverage area of mobile networks can be greatly extended by jointly using the proposed precoders and the cylindrical array antenna that achieves the service area radius of 100 km.

REFERENCES

[1] Y. Zeng, Q. Wu, and R. Zhang, "Accessing from the sky: A tutorial on UAV communications for 5G and beyond," *Proc. IEEE*, vol. 107, no. 12, pp. 2327–2375, Feb. 2019.

[2] G. Karabulut Kurt, M. G. Khoshkholgh, S. Alfattani, A. Ibrahim, T. S. J. Darwish, M. S. Alam, H. Yanikomeroglu, and A. Yongacoglu, "A vision and framework for the high altitude platform station (HAPS) networks of the future," *IEEE Commun. Surveys Tuts.*, vol. 23, no. 2, pp. 729–779, 2nd Quart., 2021.

[3] S. Karapantazis and F. Pavlidou, "Broadband communications via high-altitude platforms: A survey," *IEEE Commun. Surveys Tuts.*, vol. 7, no. 1, pp. 2–31, 1st Quart., 2005.

[4] *HAPSMobile and Loon First in the World to Deliver LTE Connectivity From a Fixed-Wing Autonomous Aircraft in the Stratosphere*. Accessed: Oct. 8, 2020. [Online]. Available: https://www.hapsmobile.com/en/news/press/2020/20201008_02/

[5] *Airbus Zephyr Solar High Altitude Platform System (HAPS) Reaches New Heights in Its Successful 2021 Summer Test Flights*. Accessed: Oct. 11, 2021. [Online]. Available: https://www.airbus.com/en/newsroom/press-releases/2021-10-airbus-zephyr-solar-high-altitude-platform-system-haps-reaches-new

[6] Q. Xi, C. He, L. Jiang, J. Tian, and Y. Shen, "Capacity analysis of massive MIMO on high altitude platforms," in *Proc. IEEE Global Commun. Conf. (GLOBECOM)*, Washington, DC, USA, Dec. 2016, pp. 1–6.

[7] Y. Wang, X. Xia, K. Xu, Y. Xu, and A. Liu, "Location-assisted precoding for three-dimension massive MIMO in air-to-ground transmission," in *Proc. IEEE Conf. Comput. Commun. Workshops (INFOCOM WKSHPS)*, Atlanta, GA, USA, May 2017, pp. 337–342.

[8] ITU-R Preparatory Studies for WRC-23, RESOLUTION 247 (WRC-19), *Facilitating Mobile Connectivity in Certain Frequency Bands Below 2.7 GHz Using High-Altitude Platform Stations as International Mobile Telecommunications Base Stations*, 2019, pp. 295–297. [Online]. Available: https://www.itu.int/dms_pub/itu-r/oth/0C/0A/R0C0A00000F0085PDFE.pdf

[9] K. Tashiro, K. Hoshino, and A. Nagate, "Cylindrical massive MIMO system for HAPS: Capacity enhancement and coverage extension," in *Proc. IEEE 93rd Veh. Technol. Conf. (VTC-Spring)*, Helsinki, Finland, Apr. 2021, pp. 1–6.

[10] Y. Shibata, N. Kanazawa, M. Konishi, K. Hoshino, Y. Ohta, and A. Nagate, "System design of gigabit HAPS mobile communications," *IEEE Access*, vol. 8, pp. 157995–158007, 2020.

[11] Z. Peng and D. Grace, "Coexistence performance of high-altitude platform and terrestrial systems using gigabit communication links to serve specialist users," *EURASIP J. Wireless Commun. Netw.*, vol. 2008, no. 1, Aug. 2008, Art. no. 892512.

[12] D. Grace, J. Thornton, G. Chen, G. P. White, and T. C. Tozer, "Improving the system capacity of broadband services using multiple high-altitude platforms," *IEEE Trans. Wireless Commun.*, vol. 4, no. 2, pp. 700–709, Mar. 2005.

[13] M. Konishi, T. Nishimaki, Y. Shibata, S. Nabatame, and A. Nagate, "A study of co-channel spectrum-sharing system between HAPS and terrestrial mobile communication networks," in *Proc. IEEE 91st Veh. Technol. Conf. (VTC-Spring)*, Antwerp, Belgium, May 2020, pp. 1–5.

[14] M. Konishi, T. Nishimaki, Y. Shibata, S. Nabatame, and A. Nagate, "An experimental study of uplink co-channel spectrum-sharing system between HAPS and terrestrial mobile communication networks," in *Proc. IEEE 92nd Veh. Technol. Conf. (VTC-Fall)*, Victoria, BC, Canada, Nov. 2020, pp. 1–5.

[15] J.-W. Lim, H.-S. Jo, H.-G. Yoon, and J.-G. Yook, "Interference mitigation technique for the sharing between IMT-advanced and fixed satellite service," *J. Commun. Netw.*, vol. 9, no. 2, pp. 159–166, Jun. 2007.

[16] M. Srinivasan, S. Gopi, S. Kalyani, X. Huang, and L. Hanzo, "Airplane-aided integrated next-generation networking," *IEEE Trans. Veh. Technol.*, vol. 70, no. 9, pp. 9345–9354, Sep. 2021.

[17] Y. Hu, Y. Hong, and J. Evans, "Modelling interference in high altitude platforms with 3D LoS massive MIMO," in *Proc. IEEE Int. Conf. Commun. (ICC)*, Kuala Lumpur, Malaysia, May 2016, pp. 1–6.

[18] S. Ananth, B. Wojtowicz, A. Cohen, N. Gulia, A. Bhattacharya, and B. Fox, "System design of the physical layer for Loon's high-altitude platform," *EURASIP J. Wireless Commun. Netw.*, vol. 2019, no. 170, pp. 1–17, Jun. 2019, Art. no. 170.

[19] J.-M. Park, D.-S. Oh, Y.-S. Kim, and D.-S. Ahn, "Evaluation of interference effect into cellular system from high altitude platform station to provide IMT-2000 service," in *Proc. IEEE Global Commun. Conf. (GLOBECOM)*, San Francisco, CA, USA, Dec. 2003, pp. 420–424.

[20] D. Zhou, S. Gao, R. Liu, F. Gao, and M. Guizani, "Overview of development and regulatory aspects of high altitude platform system," *Intell. Converged Netw.*, vol. 1, no. 1, pp. 58–78, Jun. 2020.

[21] H. Sung, S. R. Lee, and I. Lee, "Generalized channel inversion methods for multiuser MIMO systems," *IEEE Trans. Commun.*, vol. 57, no. 11, pp. 3489–3499, Nov. 2009.

[22] R. Chopra, C. R. Murthy, H. A. Suraweera, and E. G. Larsson, "Blind channel estimation for downlink massive MIMO systems with imperfect channel reciprocity," *IEEE Trans. Signal Process.*, vol. 68, pp. 3132–3145, 2020.

[23] R. Ahmed, K. Jayasinghe, and T. Wild, "Comparison of explicit CSI feedback schemes for 5G new radio," in *Proc. IEEE 89th Veh. Technol. Conf. (VTC-Spring)*, Kuala Lumpur, Malaysia, Apr. 2019, pp. 1–5.

[24] E. T. Michailidis and A. G. Kanatas, "Three-dimensional HAP-MIMO channels: Modeling and analysis of space-time correlation," *IEEE Trans. Veh. Technol.*, vol. 59, no. 5, pp. 2232–2242, Jun. 2010.

[25] M. Hata, "Empirical formula for propagation loss in land mobile radio services," *IEEE Trans. Veh. Technol.*, vol. 29, no. 3, pp. 317–325, Aug. 1980.

[26] E. Damosso and L. M. Correia, "COST action 231: Digital mobile radio towards future generation system, final report," Eur. Communities, Brussels, Belgium, Tech. Rep. EUR 18957, 1999. [Online]. Available: https://op.europa.eu/en/publication-detail/-/publication/f2f42003-4028-4496-af95-beaa38fd475f

[27] C. Zhang, Y. Jing, Y. Huang, and L. Yang, "Performance analysis for massive MIMO downlink with low complexity approximate zero-forcing precoding," *IEEE Trans. Commun.*, vol. 66, no. 9, pp. 3848–3864, Sep. 2018.

[28] J. Zhang, X. Yu, and K. B. Letaief, "Hybrid beamforming for 5G and beyond millimeter-wave systems: A holistic view," *IEEE Open J. Commun. Soc.*, vol. 1, pp. 77–91, 2020.

[29] K. Tashiro, K. Hoshino, and A. Nagate, "Cylindrical massive MIMO system with low-complexity angle-based user selection for high-altitude platform stations," *IEICE Trans. Commun.*, vol. 105, no. 4, pp. 449–460, Apr. 2022.

[30] *5G; Study on Channel Model for Frequencies From 0.5 to 100 GHz*, 3GPP document TR 38.901, version 14.3.0 Release 14, Jan. 2018.

[31] *Universal Mobile Telecommunications System (UMTS); Spatial Channel Model for Multiple Input Multiple Output (MIMO) Simulations*, 3GPP document TR 25.996, version 13.0.0 Release 13, Sep. 2020.

[32] M. Mikami, S. Maiti, and H. Yoshino, "Cell identification performance optimization in co-channel heterogeneous cellular networks employing CRE based on a hierarchical synchronization signal structure," in *Proc. IEEE 83rd Veh. Technol. Conf. (VTC Spring)*, Nanjing, China, May 2016, pp. 1–5.

[33] Y. Jiang, M. K. Varanasi, and J. Li, "Performance analysis of ZF and MMSE equalizers for MIMO systems: An in-depth study of the high SNR regime," *IEEE Trans. Inf. Theory*, vol. 57, no. 4, pp. 2008–2026, Apr. 2011.

[34] A. Goldsmith, S. A. Jafar, N. Jindal, and S. Vishwanath, "Capacity limits of MIMO channels," *IEEE J. Sel. Areas Commun.*, vol. 21, no. 5, pp. 684–702, Jun. 2003.

[35] A. Chiumento, M. Bennis, C. Desset, L. V. der Perre, and S. Pollin, "Adaptive CSI and feedback estimation in LTE and beyond: A Gaussian process regression approach," *EURASIP J. Wireless Commun. Netw.*, vol. 2015, no. 168, pp. 1–14, Jun. 2015, Art. no. 168.

KOJI TASHIRO (Member, IEEE) received the B.E., M.E., and Ph.D. degrees from the Kyushu Institute of Technology, Fukuoka, Japan, in 2014, 2016, and 2019, respectively. From 2018 to 2020, he was with the Kyushu Institute of Technology as a Research Fellow of the Japan Society for the Promotion of Science (JSPS). Since 2020, he has been with the Technology Research Laboratory, SoftBank Corporation. His research interests include array antenna techniques as well as signal processing in MIMO communications. He is a member of the IEICE. He received the Best Paper Award from IEICE in 2021.

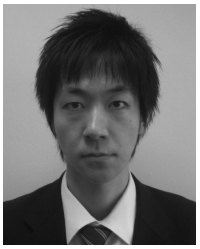

KENJI HOSHINO received the M.E. degree in information engineering from the Shibaura Institute of Technology, in 2007, and the Ph.D. degree from the Tokyo Institute of Technology, in 2021. He joined SoftBank Telecom Corporation (currently, SoftBank Corporation), in 2007, and engaged in research and development of mobile communication systems. Since 2015, he has been a Research Engineer at SoftBank Corporation. From 2017 to 2021, he worked as a Research Engineer at HAPSMobile Inc. His current interests include wireless transmission and adaptive array antenna technologies for mobile communication systems. He is a member of the IEICE. He received the Academic Encouragement Award from IEICE in 2012.

ATSUSHI NAGATE (Member, IEEE) received the M.E. and Ph.D. degrees from Osaka University, in 2001 and 2016, respectively. He joined Japan Telecom Company Ltd. (currently, SoftBank Corporation), in 2001, and has been engaged in research and development of mobile communication systems. He is currently a Senior Director of the Technology Research Laboratory, SoftBank Corporation. His research interests include mobile communications and UAV communications. He is a member of the IEICE.